INTERNATIONAL ATOMIC ENERGY AGENCY
UNITED NATIONS EDUCATIONAL, SCIENTIFIC AND CULTURAL ORGANIZATION

INTERNATIONAL CENTRE FOR THEORETICAL PHYSICS
34100 TRIESTE (ITALY) - P.O.B. 586 - MIRAMARE - STRADA COSTIERA 11 - TELEPHONES: 224281/2/3/4/5/6
CABLE: CENTRATOM - TELEX 460392-I

SMR/113 - 27

AUTUMN COLLEGE

ON

THE TROPOSPHERE, STRATOSPHERE AND MESOSPHERE

10 September - 19 October 1984

MIDDLE ATMOSPHERE PROGRAM

A.P. MITRA

National Physics Laboratory
Hillside Road
New Delhi 110012
India

1. The Middle Atmosphere Program (MAP), designed to study the region between the tropopause and the mesopause, started on January 1, 1982 and will continue through December 31, 1985. It is a successor to the IGY, IQSY and the IMS and is operated and managed by the MAP Steering Committee set up by SCOSTEP. This portion of the atmosphere (roughly 10-85 km) had in the past been only inadequately studied. Participating countries are many, but few from developing countries or from tropical regions.

2. The genesis, objectives and, goals and perspectives of the program are outlined. In recent years new techniques have been introduced for the detection of minor species (present in quantities from a few parts per million to a few parts per trillion) and of motions in the atmosphere. These include the MST radar (still under construction in several cases), LIDAR, laser heterodyning system, high resolution spectroscopy and the increasing use of atmospheric remote sensing from satellites.

3. MAP had a few Pre-MAP activities (PMP series) and have currently a number of projects. Some initial results are indicated. Of considerable interest are the coordinated balloon or rocket intercomparison programs: the balloon windy vapour program, the rocket ozone intercomparison programs etc.

WHY MAP ?

Three main goals :

- What are possibilities of damage to earth's middle atmosphere from man's activities
  eg. Ozone problem
- What role does middle atmosphere play in determining climate and climatic changes ?
- What are the processes by which the sun, acting through the middle atmosphere, may be able to affect weather ?
  : Sun-weather Relationship

Why MAP NOW ?

- NEW TECHNIQUES
  - ST/MST RADARS
  - METEOR RADAR
  - PR RADAR
  - LIDAR – LASER HETERODYNING
  - HIGH RESOLUTION SPECTROSCOPY
  - AVAILABILITY OF NETWORK OF SATELLITES
  - BALLOON, ROCKET SENSORS
- AWARENESS OF ROLE OF MA. IN DAMAGE TO OZONE ENVIRONMENT AND IN STP-M
- INCREASING MODELLING CAPABILITY WITH LARGE COMPUTERS
- NEED FOR GLOBAL COORDINATION

PROGRAMME SPECIFICS

- THERMAL STRUCTURE AND CHANGES
  (Special situations like Cold Mesopause, Stratospheric Warming)

- COMPOSITION AND ATMOSPHERIC CHEMISTRY
  (MINOR SPECIES RELEVANT IN OZONE CHEMISTRY
  GREENHOUSE MOLECULES)

- INTERACTION OF:
  RADIATION FROM SUN, EARTH, ATMOSPHERE
  WITH
  MIDDLE ATMOSPHERE

- MONITORING OF MOTIONS OF ALL SCALES

AMP

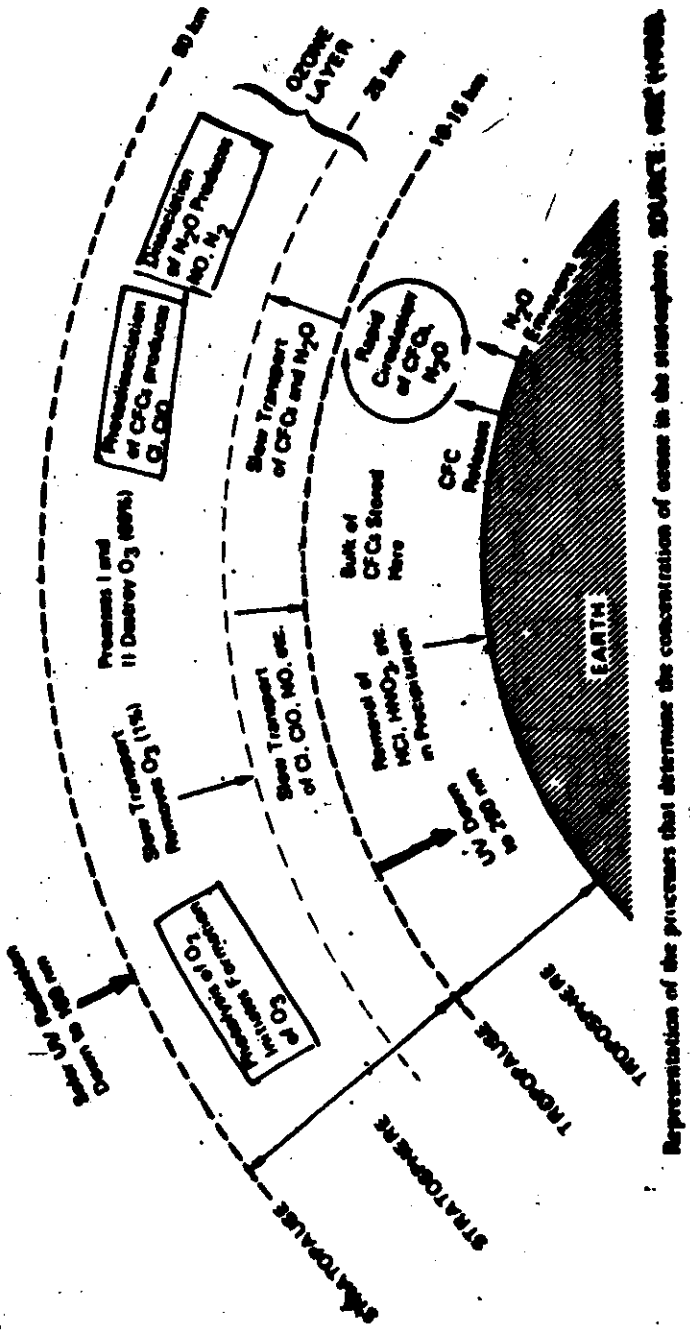

Representation of the processes that determine the concentration of ozone in the atmosphere. SOURCE: WMO (1988)

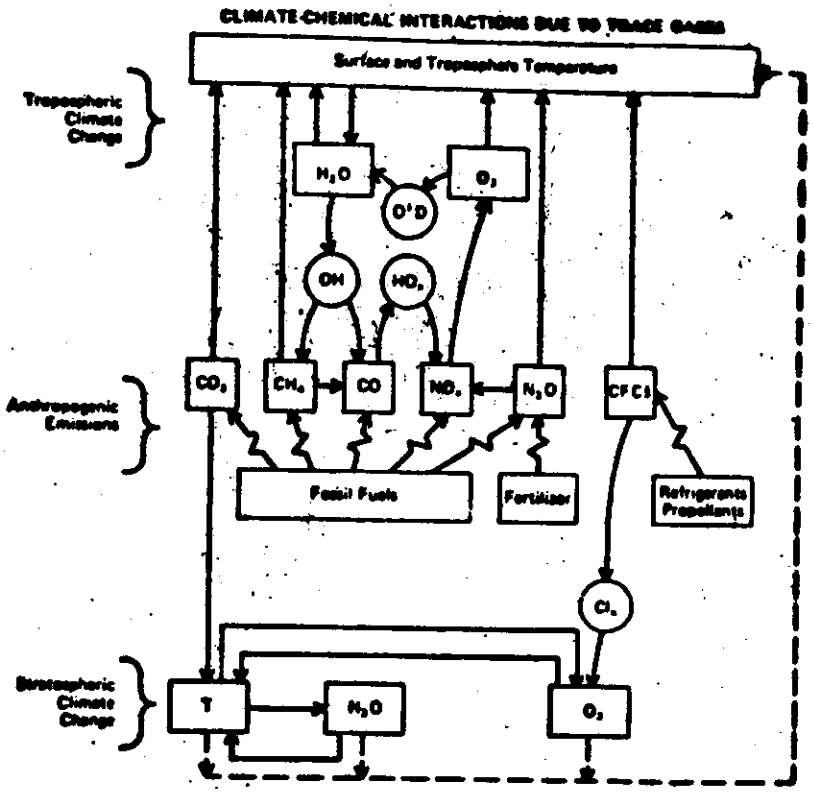

. *Climate-chemical interactions due to trace gases. (Source: Ramanathan, V., 1980: Climate effects of anthropogenic trace gases. Interactions of Energy and Climate. D. Reidel Publishing Company. pp. 269-280.)*

APPLICATIONS

1 THREATS TO OZONE LAYER FROM HUMAN ACTIVITIES

2 EFFECTS OF STRATOSPHERIC CHANGES IN SURFACE ENVIRONMENT AND CLIMATE

3. SUN-WEATHER RELATIONSHIP

4 COMMUNICATION THROUGH QUIET AND DISTURBED D-REGION

- NAVIGATION
- AIRCRAFT COMMUNICATION, ESPECIALLY THROUGH TRANSPOLAR FLIGHTS

5. STRATOSPHERIC CATS

New Techniques

- MST/ST
- PR RADAR
- METEOR RADAR
- VHF RADAR
- MULTIWAVELENGTH RADIOMETER
- UV-B PHOTOMETER
- LIDAR
- LASER HETERODYNING
- HIGH RESOLUTION SPECTROSCOPY FROM BALLOONS & ROCKETS
- GRAB SAMPLING
- SATELLITE BASED MEASUREMENTS

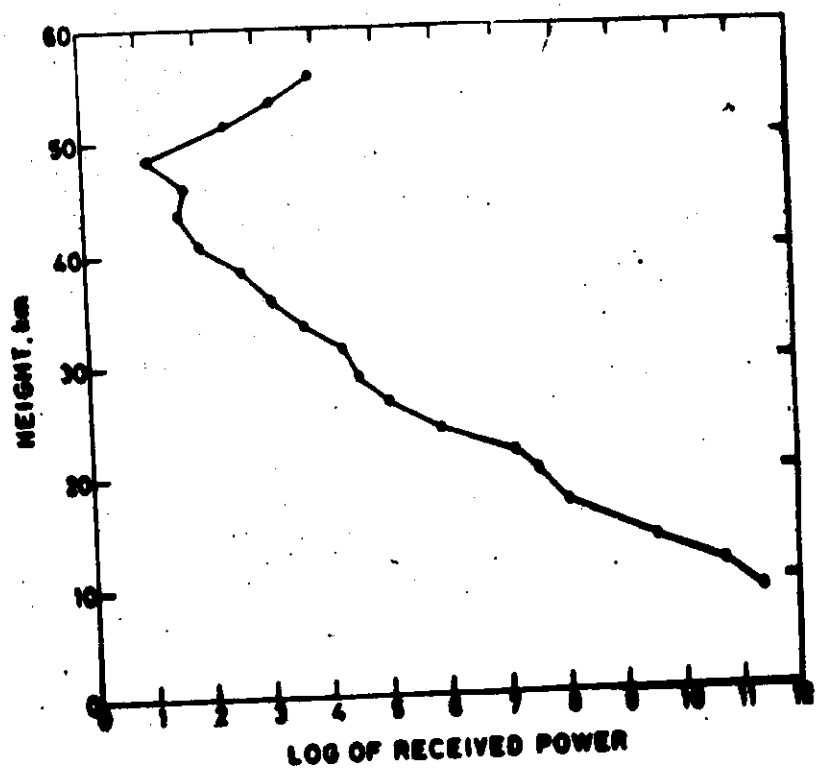

Height-variation of the received power obtained using the Jicamarca radar on 10 January 1977. The logarithms are to base ten. (After Balsley, 1978.)

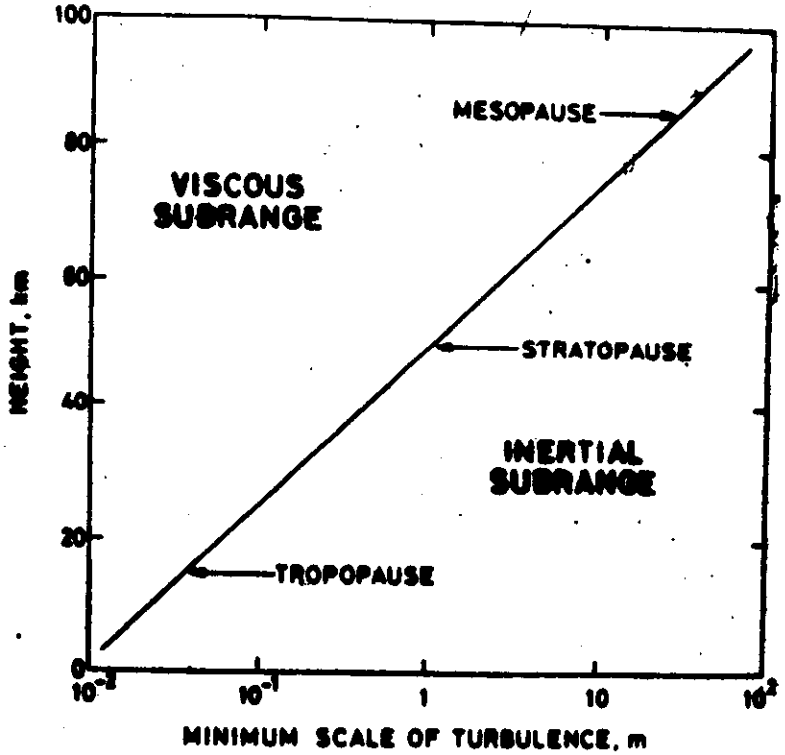

Height-variation of the minimum scale of turbulence, i.e. the lower limit of the inertial sub-range. (After Reiley and Gage, 1980.)

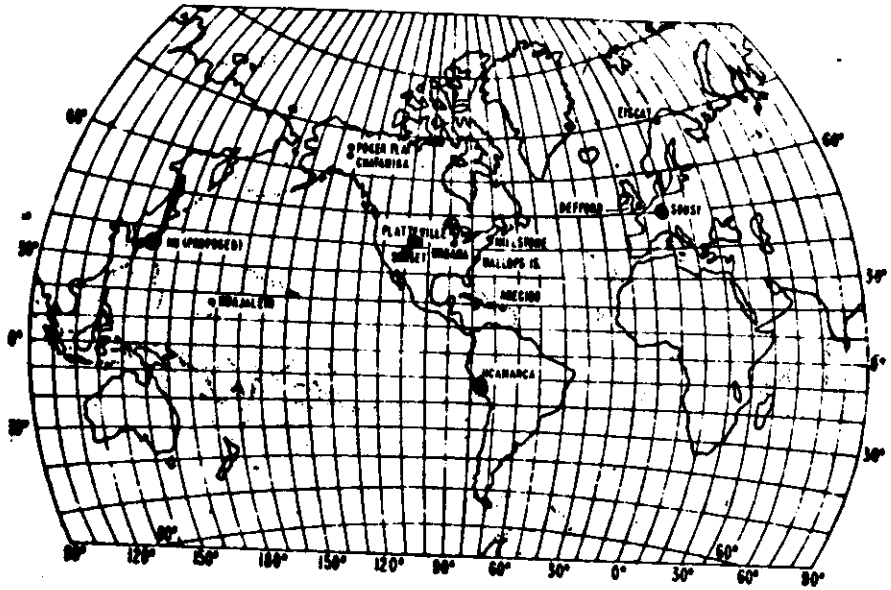

Location of various radar facilities with MST/ST capability listed in Table 1.

TABLE 1 SYSTEM PARAMETERS FOR EXISTING RADARS

Facility	Frequency (MHz)	Effective Antenna Area (m^2)	Beamwidth (°)	Beam Power Aperture (Wm^2)	Min. Range Resolution (m)	Antenna Type
Incoherent scatter facilities						
Jicamarca (Peru)	49.9	8.4×10^5	1.0	2.8×10^{10}	2500	Dipoles
Arecibo (Puerto Rico)	430	5.6×10^4	0.2	8.7×10^8	300	Dish
Chatanika (Alaska)	1290	2.2×10^2	0.6	5.8×10^7	375	Dish
EISCAT (Scandinavia)	(224 (vhf)	3.0×10^3	1.9×0.6	3.3×10^9	150	Parabolic cylinder
	(934 (uhf)	5.7×10^2	0.6	2.4×10^8	150	Dish
ST/MST facilities						
SOUSY (Germany)	53.5	3.1×10^3	5.0	7.6×10^7	100	Yagis
Sunset (Colorado)	40.5	1.8×10^3	5.0×9.0	9.4×10^6	150	Dipoles
Poker Flat (Alaska)	49.9	1.0×10^5 (4.0×10^5)	2.2 (1.1)	4.0×10^6 (2.6×10^9)	2000 (300)	Dipoles

MST

Facility	Frequency (MHz)	Effective Antenna Area (m^2)	Beamwidth (°)	Mean Power Aperture (Wm^2)	Min. Range Resolution (m)	Antenna Type
Jicamarca (Peru)	49.9	8.4×10^5	1.0	2.8×10^{10}	2500	Dipoles
Arecibo (Puerto Rico)	430	5.6×10^4	0.2	8.7×10^8	300	Dish
Chatanika (Alaska)	1290	2.2×10^2	0.6	5.8×10^7	375	Dish
EISCAT (Scandinavia)	(224 (vhf)	3.0×10^3	1.9×0.6	3.3×10^9	150	Parabolic cylinder
	(934 (uhf)	5.7×10^2	0.6	2.4×10^8	150	Dish
ST/MST facilities						
SOUSY (Germany)	53.5	3.1×10^3	5.0	7.6×10^7	100	Yagis
Sunset (Colorado)	40.5	1.8×10^3	5.0×9.0	9.4×10^6	150	Dipoles
Poker Flat (Alaska)	49.9	1.0×10^5 (4.0×10^5)	2.2 (1.1)	4.0×10^6 (2.6×10^9)	2000 (300)	Dipoles

MST

Facility	Frequency (MHz)	Effective Antenna Area (m^2)	Beamwidth (°)	Mean Power Aperture (Wm^2)	Min. Range Resolution (m)	Antenna Type
Jicamarca (Peru)	49-55	2.1×10^5	3.0	1.3×10^9	150	Dipoles
Chung-Li (Taiwan)	52	4.5×10^3	3.0	1.7×10^7	150	Yagis
Adelaide (Australia)	54	7.8×10^3	3.2	2.7×10^6	1000	Dipoles and Yagis
Britain (USA)	40.9	10^5	1.0	3×10^9	150	[illegible]
Shigaraki (Japan)	46.5	8.3×10^3	3.6	4.3×10^7	150	Yagis
UK	50	5.2×10^3	3.4	6.2×10^6	150	Yagis

PROPOSED INDIAN MST RADAR
MAIN SPECIFICATIONS

Frequency :	45-55 MHz
Bandwidth :	2 MHz ± 10%
Pulsewidth :	1-32 μs (adjustable in 1 μs steps)
PRF :	250 KHz - 8 KHz binary steps
Transmitter :	24 modules of 100 KW peak power Total power : 2.5 MW Average power: 60 KW
Antenna :	Coaxial Collinear 2.1×10^4 m² 3 deg Zenith, ± 20° E-W, ± 20° N-S
Data Processing :	Velocity Resolution : 0.1 m/s and 0.2 m/s Range resolution : 125/250 m, 500 m, 1 Km, 4 Km (selectable)
Power aperture product :	2×10^9 W m²

MUR (JAPAN)

RADAR SYSTEM	MONOSTATIC PULSE RADAR & ACTIVE PHASED ARRAY SYSTEM
OPERATIONAL FREQUENCY	46.5 MHz
TRANSMITTER	
PEAK POWER	1 MW min
Average power	50 KW min (duty ratio of 5%)
pulse length	2 - 200 μs (variable)
pulse repetition freq	2.5 KHz min. for pulselength of 2 μs (smaller for longer pulses)
ANTENNA	
Polarization	linear and circular
Aperture	circle of about 100 m. in diameter
Beam width	3.6° (full antenna)
RECEIVER	
Dynamic range	70 db min
IF bandwidth	1 MHz maximum
MASTER OSCILLATOR	rubidium vapour

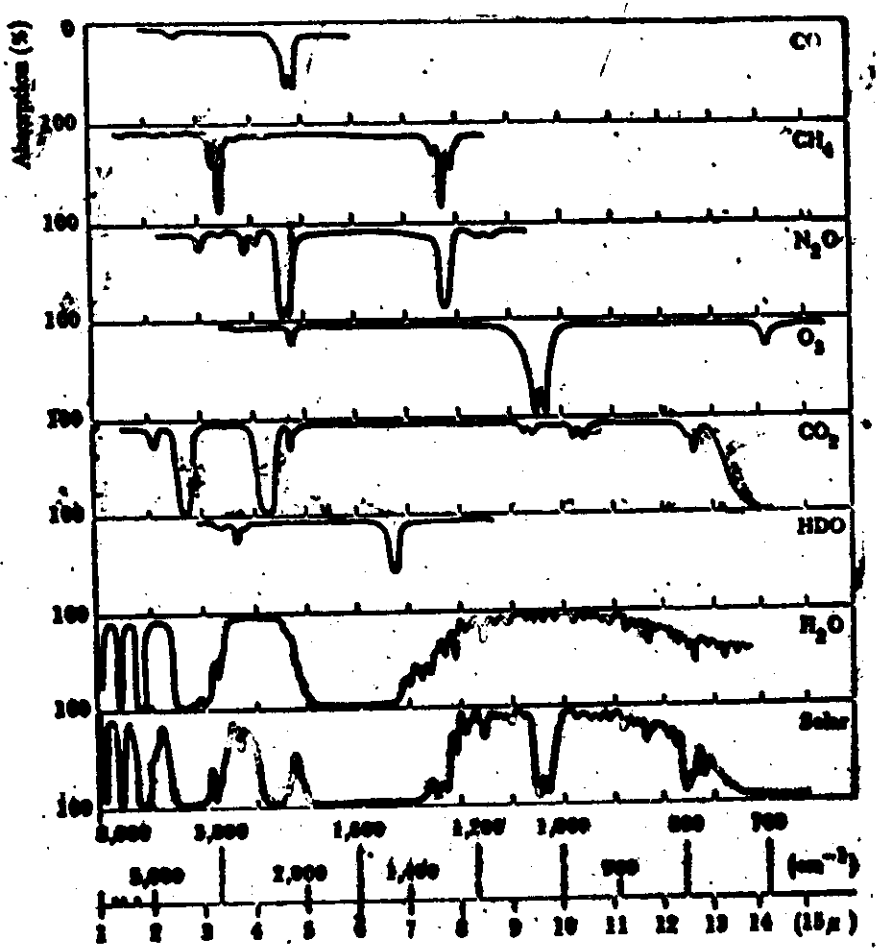

FIG. 2. Comparison of the near-infra-red solar spectrum with laboratory spectra of various atmospheric gases.

FRENCH LIDAR

LOCATION: HAUTE PROVENCE
44°N, 6°E

TYPE : Nd^{++} YAG

COVERAGE : 30 - 80 km
ABOVE 30 KM ATMOSPHERE IS CLEAN AND ONLY SCATTERING IS RAYLEIGH SCATTERING

ACQUISITION $\Delta z = 150$ m, $\Delta t = 5$ min

Typical VALUES $\Delta z = 1.2$ km, $\Delta t = 1$ hr

T ACCURACY :

0.3 K	35 km
1 K	50 km
10 K	80 km

P ACCURACY

0.1%	35 km
1%	65 km
10%	85 km

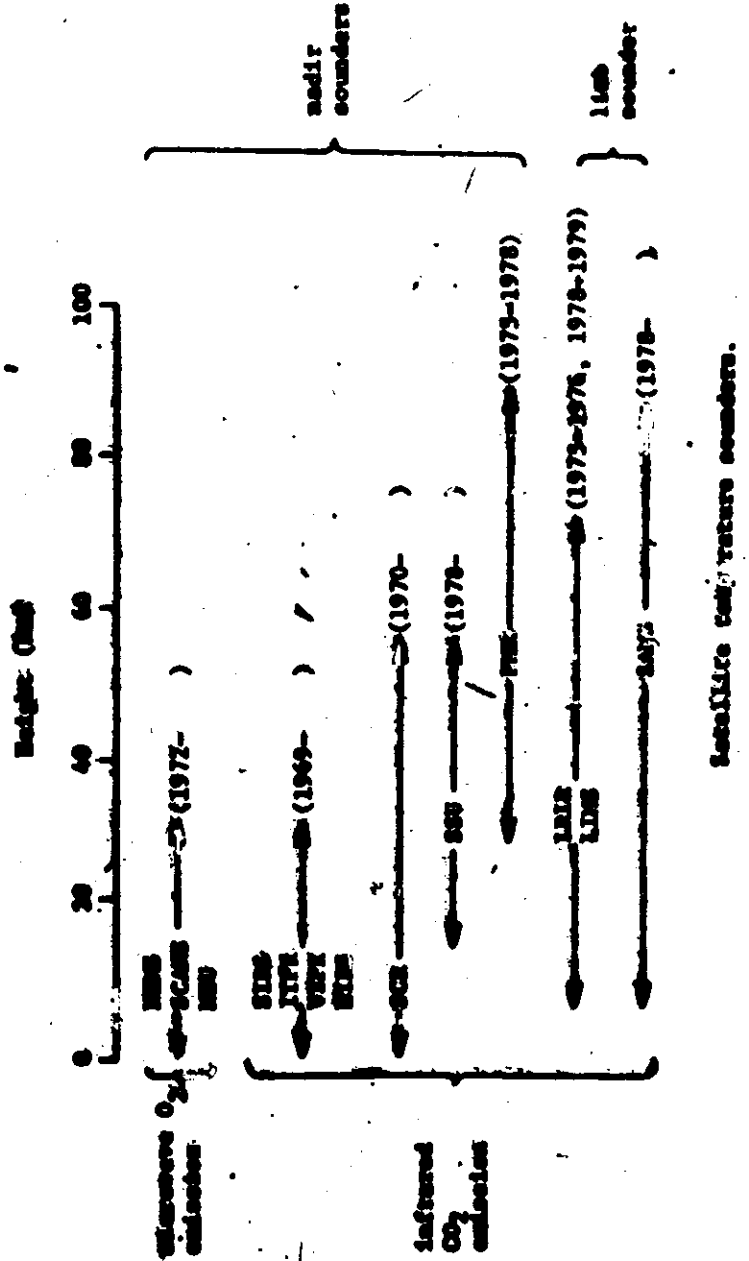

Satellite Temperature Sounders

1. A wide range of multichannel temperature sounding instruments carried by satellites since 1969

   Vertical resolution varies from:

   ~ 2 km for LIMS

   to ~ 20 km for some of 42 vertical sounds.

   Horizontal resolution varied from a few tens of kms for scanning instruments to orbital sepn. of about 2000 km.

2. Most instruments sound temp. by IR emissn from CO_2, but some microwave emission from O_2

3. In operation for different time spans

   Continuous meas. of whole stratosphere available since 1970

   Mesosphere observations since 1975

   Real time daily met. analysis 10 mb – 0.4 mb from TIROS N Satl. 1978 to 1985

   SSU, MSU, HIRS II are scanning radiometers viewing on either side of Nadir

SPECIAL OBSERVATIONAL CAMPAIGNS

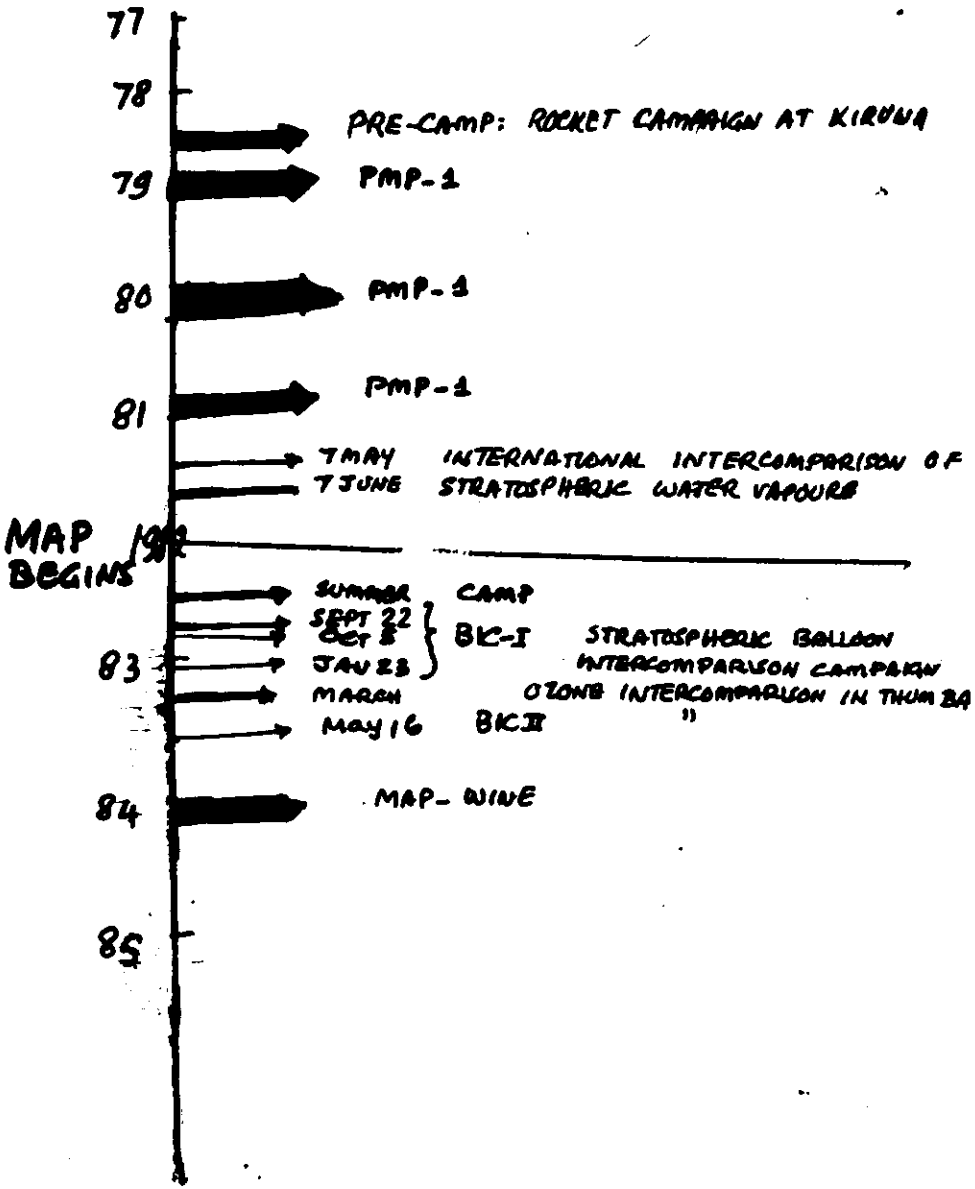

PMP-1

PMP-2

PMP-3

PRE-MAP PROJECTS

Coordinated study of the Behaviour of the Middle Atmosphere in Winter (Labitzke)

(variability; interaction of planetary scale waves of tropospheric origin with mean flow in stratosphere and mesosphere)
Use of two satellites launched during September 1978: TIROS N, ARMBUS &
WINTERS OF 1978/79, 1979/80, 1980/81

EQUATORIAL WAVE DYNAMICS (HIROTA)

(Satellite observations of planetary scale waves, coherent scatter radar observations of winds and waves, computer studies of mechanistic dynamic models in 2 and 3 dimensions and long time scales)

STUDY OF PHOTOCHEMICAL PROCESSES IN UPPER STRATOSPHERE AND MESOSPHERE BY COMPLEMENTARY SPACECRAFT, IN SITU, & GROUND MEASUREMENTS (J.C. GILLE)

(combined use of several techniques and development of a uniform standard for intercomparison of data); use of data from satellite experiments such as SAGE, SAM, SAM II, LIMS); future satellites planned to be used: SME (Solar Mesosphere Explorer), Dynamics Explorer, SAGE (Aerosols, O_3, NO_2), HALOE, SPACELABS I and III, UARS.

MP-4 METEOROLOGICAL AND CHEMICAL VARIABLES IN FORMAT OF MONTHLY MEAN ZONAL CROSSSECTIONS (BURNETT)

MP-5 Solar Spectral Irradiance Measurements (Simon).
(Temporal variation of solar ultraviolet irradiance).

STUDY GROUPS

SG-1 TROPOSPHERE - STRATOSPHERE COUPLING. CHEMICAL & DYNAMICAL (HOLTON)

SG-2 TRANSPORT OF TRACE CONSTITUENTS (MAHLMAN)

MSG-3 TIDES, GRAVITY WAVES & TURBULENCE (GELLER)

MSG-4 ELECTRODYNAMICS OF THE MIDDLE ATMOSPHERE (VOLLAND)

MSG-5 IONS AND AEROSOLS (ARNOLD)
(Review and Evaluate theoretical and experimental studies involving atmospheric ions and their relationship to neutral gases and aerosols)

MSG-6 SCIENTIFIC ASPECTS OF AN INTERNATIONAL EQUATORIAL OBSERVATORY (KATO)
(Proposal for establishment of an international equatorial middle atmospheric observatory)

MSG-7 PENETRATION OF SOLAR RADIATION INTO THE ATMOSPHERE (FREDERICK)
(Review and evaluate solar irradiance in the middle atmosphere including the range 175 nm to visible

MSG-8 ATMOSPHERIC CHEMISTRY (WITT)
(Review and evaluate theoretical and experimental studies of middle atmospheric chemical composition and to identify areas of further research).

MSG-9 MEASUREMENT OF MIDDLE ATMOSPHERE PARAMETERS BY LONG DURATION BALLOON FLIGHTS (BLAMONT)
(Long duration circumpolar balloon flights)

MAP PROJECTS

AMA : ANTARCTIC MIDDLE ATMOSPHERE (HIRASAWA)
(Coordinate investigations of dynamics, structure, composition, particle precipitation, middle atmosphere - low atmosphere interactions, atm. pollution; northern-southern polar atm-comparison)

ATMAP : ATMOSPHERIC TIDES (FORBES)
(To facilitate interaction between observationalists, data analysts, theoreticians & modellers & study tides on a global scale)

CAMP : COLD ARCTIC MESOPAUSE PROJECT (Björn)
(Formation of noctilucent clouds & ozone and chemistry at low temperatures)

CLIMAT :

DYNAMICS: Dynamics of the Middle Atmosphere (LABITZKE)
in Winter - Coordinated Studies
(emphasis on disturbed winter conditions)

GLOBMET : GLOBAL METEOR OBSERVATION SYSTEM (ROPER)

GLOBUS : GLOBAL BUDGET OF STRATOSPHERIC TRACE CONSTITUENTS (SCHILER) → (FFERMAN)
(To coordinate the integrated campaign for global ozone measurements) (McCORMICK)

GOSSA : GLOBAL OBSERVATION AND STUDY OF STRATOSPHERIC AEROSOLS
(coordination; communicate data and instruments)

GRATMAP : GRAVITY WAVES & TURBULENCE (GJELLER)
(Global morphology of, theoretical geographical & seasonal trends.

MAE : MIDDLE ATMOSPHERE ELECTRODYNAMICS (MAYNARD)
(Basic physical/chemical processes, sources, nature of coupling)

SSIM : SOLAR SPECTRAL IRRADIANCE (SIMON)
MEASUREMENTS
(calibration, reference scale)

WINE : WINTER IN NORTHERN EUROPE (VON ZAHN)
(Year to variability of structure, motion and composition)

OZMAP Observations of Sources of Spatial and Temporal Variability of OZONE in Middle Atmosphere on Climatological Time Scale (HEATH)
(Preparation of daily synoptic maps of global ozone fields as basis for 3-dimensional ozone climatology)

MACWACS METEOROLOGICAL AND CHEMICAL VARIABLES AS ZONAL AVERAGED CROSS SECTIONS (RUSSELL)
(In 4i form of monthly mean zonal cross sections)

SWAMP STRATWARM MESOSPHERIC PROJECT
(Sub-project of DYNAMICS)
(To coordinate observational studies of M.A composition and dynamics during a stratospheric warming in Europe).

PARTICIPATING COUNTRIES

EUROPEAN REGION

Belgium
Czechoslovakia
Finland
France
FRG
GDR
Spain
Hungary
Ireland
Italy
Norway
Sweden
UK
USSR

ASIAN REGION

India
Israel
Japan
Taiwan
USSR

AMERICAN REGION

Canada
USA
Argentina

Southern Hemisphere

Australia
Argentina
New Zealand

MAP-2-2

MST

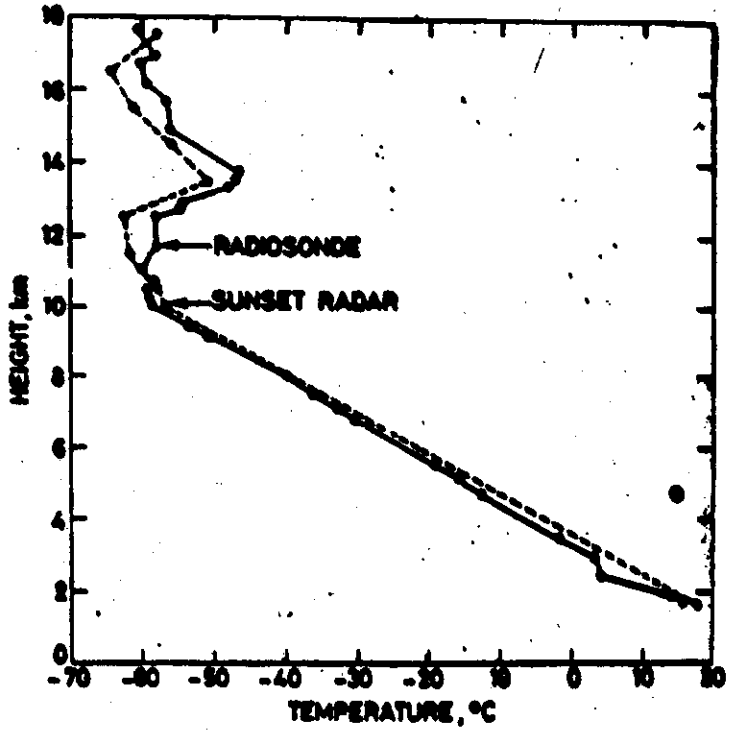

Temperature profiles for 00 UT on 26 March 1977 obtained by means of the Sunset radar and from the Denver radiosonde observations. (After Gage and Green, 1982.)

MSF

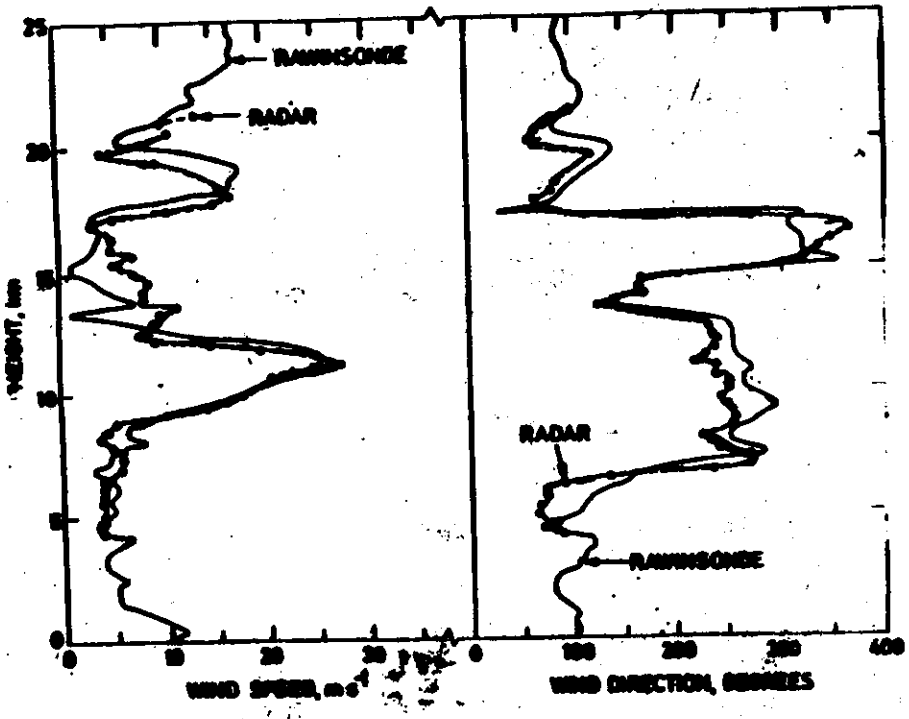

Vertical profiles of wind speed and direction measured by the Arecibo radar on 6 April 1977 compared with almost simultaneous rawinsonde observations from San Juan, Puerto Rico. (After Pacing et al., 1979.)

CAMP RESULTS

Campaigns
1. July/August 1978
2. SUMMER 1982

Results

1 Existence of thin layers (~0.5-1Km) at 91-96.5km with heavy positive ions, identified as $H^+(H_2O)_n$, with mass range 55-350 AMU

2. Low and Variable mesospheric temperature between 140K at 83 Km and 116K at 94Km

3. Evidence of presence of negatively charged aerosol particles between 82-90Km with surface area of above 6×10^{-9} cm^2/cm^3, interpreted as ice particles on July 30, 1978

4. Low and variable density of O ($\sim 10^{10}$ cm^{-3}) and NO ($\sim 10^6$ cm^{-3}) below 92Km on July 30, 1978

5. H_2O mixing ratio 2-6 ppmv in mesosphere between 80-90 Km

6. H_2O_2 mixing ratios of 0.13 ppbv at 84.3 Km on Aug 13, 1978

7. Persistent polar mesosphere cloud layer observed from SME satellite, 80-85 Km; with thickness of 3.6 Km.
Particles in cloud are probably ice aerosols of $r < 0.07\,\mu m$. Lifetime of ~1day. Upper limit of water content of ice particles ~ 1.5 mg/m^3 (~ 15 ppmv

OZONE INTERCOMPARISON CAMPAIGN IN THUMBA

A. ROCKET FLIGHTS

1. Central Aerological Observatory, USSR — Soviet optical ozonometer; Soviet chemical ozonometer
2. Physical Research Lab, Ahmedabad — Solar UV photometer and lunar ultraviolet photometer
3. National Physical Laboratory, New Delhi — 2-Channel photometer

B. BALLOONS

India Meteorological Dept. — Balloon ozonesonde and radiosonde

C. GROUND OBSERVATIONS

1. India Met. Dept. — Dobson; Surface ozone observation
2. Indian Institute of Tropical Meteorology — Photometric observation of the sun for total ozone monitoring

MAP 2-11

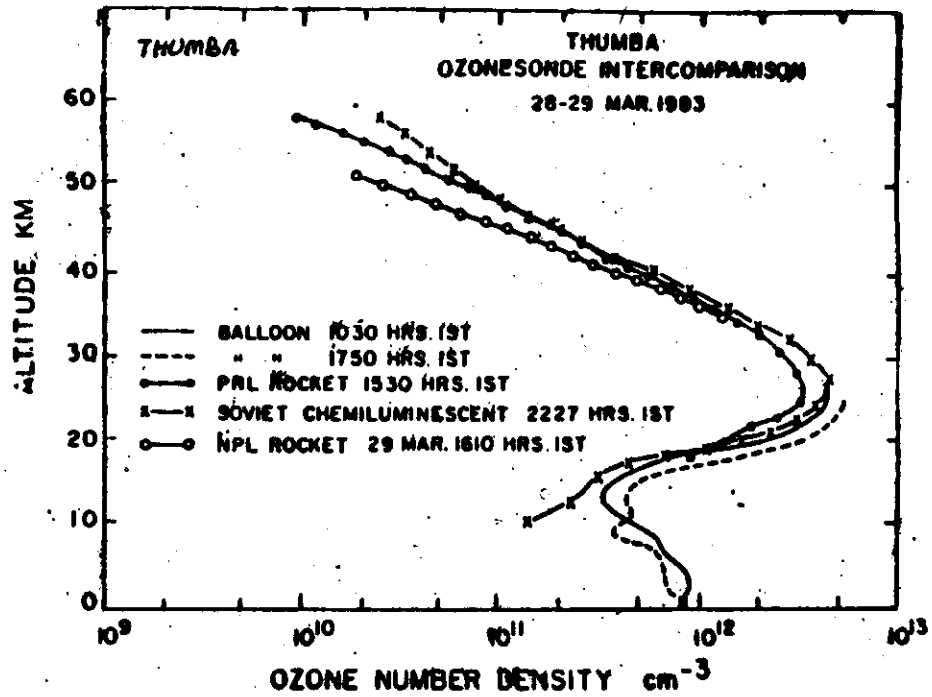

MAP 2-13

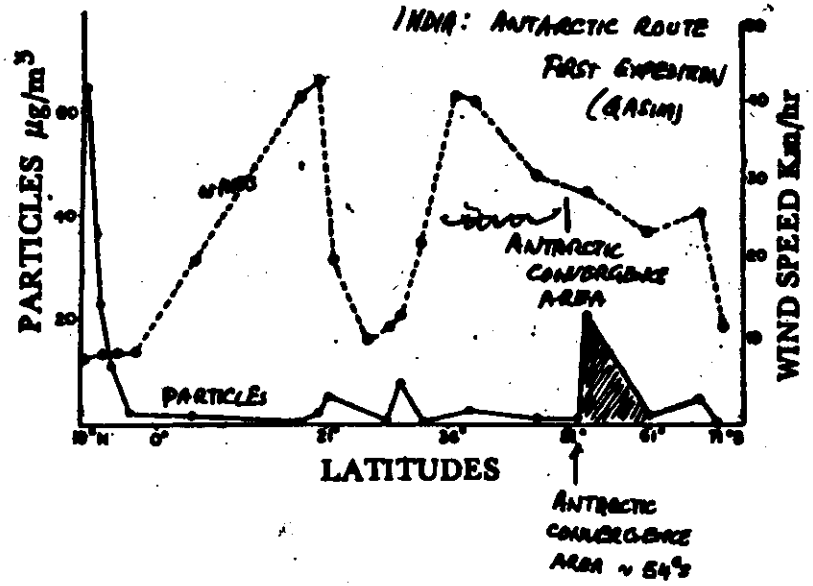

MAP 2-13

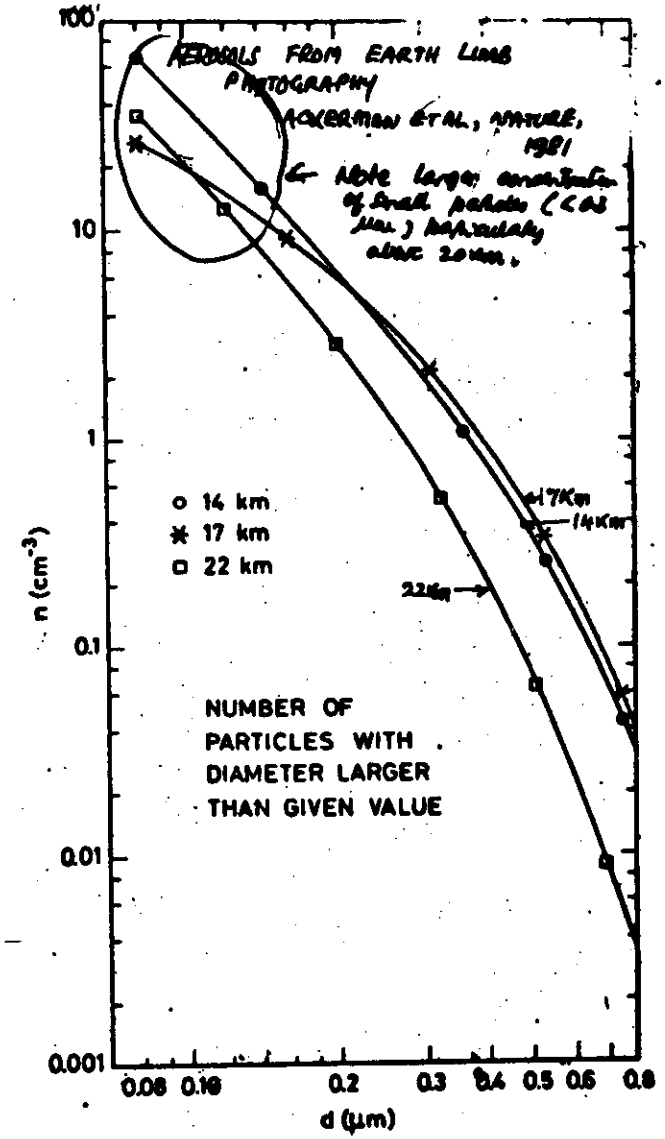

MAP-2-8

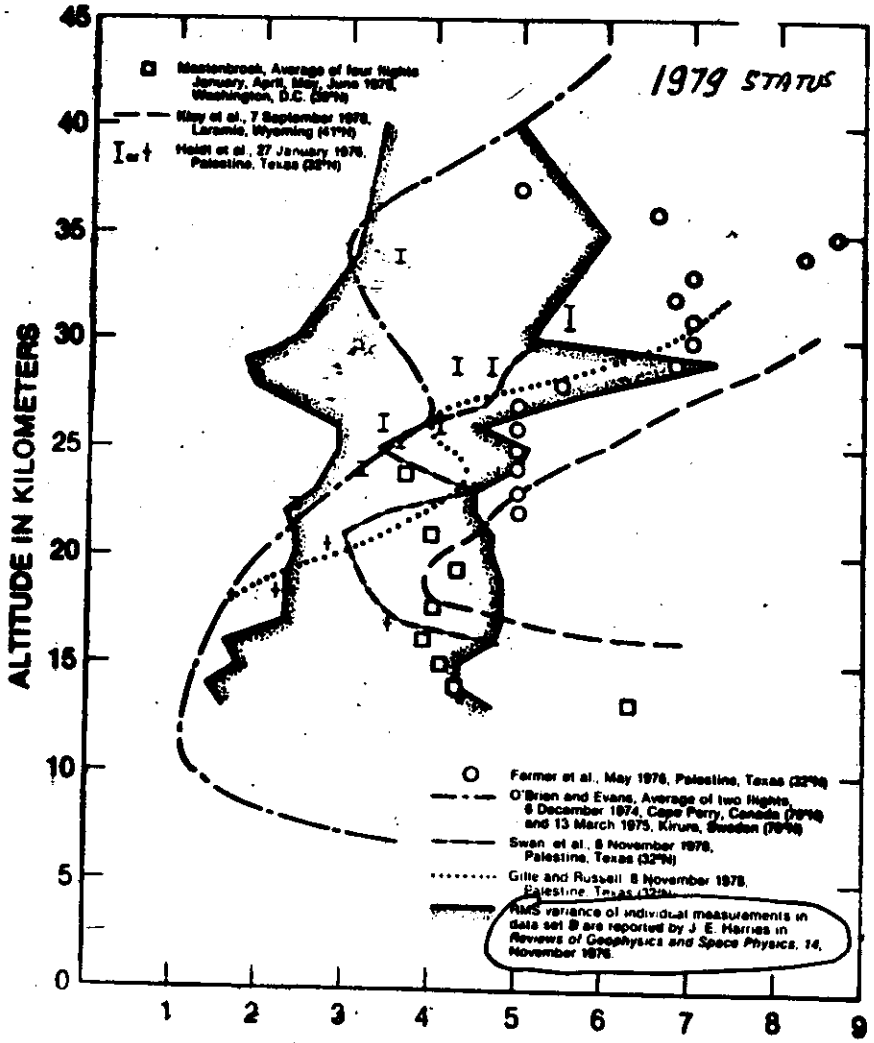

STRATOSPHERIC WATER VAPOUR PROFILES FROM SEVEN SOURCES

MAP-2-9

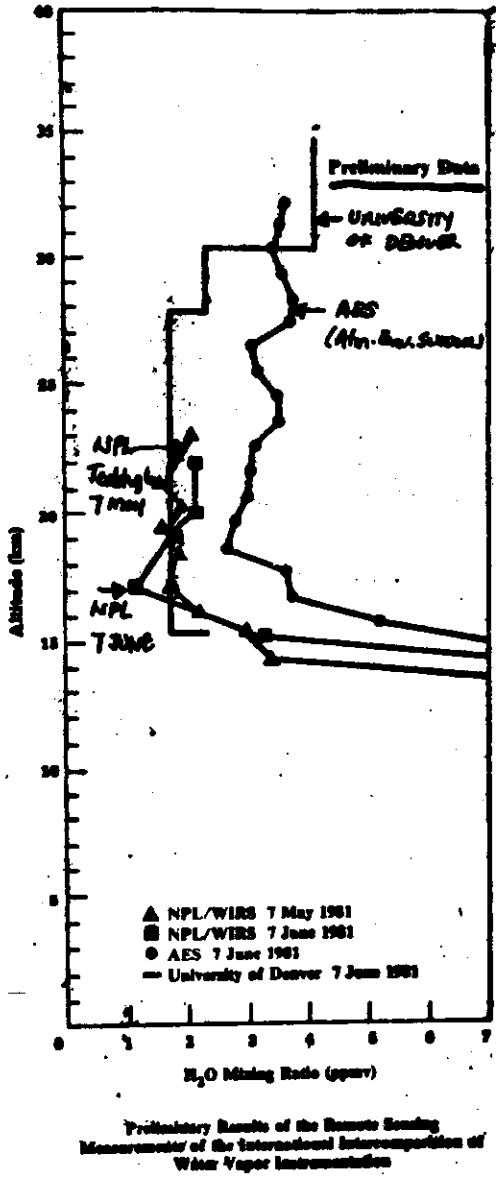

Preliminary Results of the Remote Sensing Measurements of the International Intercomparison of Water Vapor Instrumentation

International Intercomparison of Stratospheric Water Vapour

AES : Scanning Radiometer

NPL : Water Vapour IR Radiometer Sonde

Denver : Emission Spectrometer

All launches on University of Denver Gondola.

MAJOR OBJECTIVES OF BALLOON INTERCOMPARISON CAMPAIGN

1. ASSESS ACCURACY OF INSTRUMENTS CURRENTLY USED TO OBTAIN DATA ON STRATOSPHERIC MINOR SPECIES

2. OBTAIN A COMPREHENSIVE DATA SET OF KNOWN ACCURACY TO TEST THEORETICAL MODELS OF STRATOSPHERIC PHOTOCHEMISTRY

TASKS

1. Evaluate accuracy of measurements by intercomparing data from a large collection of remote sensing instruments (absorption, emission, spectrometric, radiometric...)

2. Complement balloon measurements with supporting measurements (ground based, aircraft) to compare column abundances

3. Dataset for a number of key atmospheric species

   Main intercomparison : HCl, HF, HNO_3 } Principal reservoirs for stratospheric chlorine, fluorine and nitrogen

   Subsidiary : NO, NO_2

4. Associated measurements of solar UV radiation, stratospheric T, p, winds needed for optimum analysis.

TABLE 2
MILESTONES OF
BALLOON INTERCOMPARISON CAMPAIGNS

BIC-1

SEPTEMBER 22, 1982 : 4 LAUNCHES BY PAIRS; SUCCESSFUL
3 PAYLOADS AT MEAN ALTITUDE OF 40 KM
(JPL # 2, AES, LIEGE)
1 BALLOON FAILURE ON ASCENT (NPL)
OBSERVATIONS DURING SEPT. 22, PM AND SEPT. 23, AM
CUT-DOWN AND RECOVERIES, OK.

OCTOBER 5, 1982 : SOLO-FLIGHT OF NPL GONDOLA
FLOAT ALTITUDE ~ 30 KM
OBSERVATIONS DURING OCT. 5, PM AND OCT. 6, AM
CUT-DOWN AND RECOVERY, OK.

JANUARY 23, 1983 : SOLO-FLIGHT OF SAO-FAR IR EMISSION FTS
FLOAT ALTITUDE ~ 36.5 KM
CUT-DOWN AND RECOVERY, OK.

BIC-2

MAY 16, 1983 : 2 SIMULTANEOUS LAUNCHES
1 BALLOON FAILURE ON RELEASE (NPL)
1 " " AT 20 KM ALTIT. (JPL # 1)
HEAVY DAMAGES ON BOTH PAYLOADS.

MEMORANDUM TO INVESTIGATE BALLOON FAILURES !

JUNE 17, 1983 : 2 SIMULTANEOUS LAUNCHES, SUCCESSFUL (JPL#2 AND LIEGE)
[2D. PAIR OF PAYLOADS DELAYED (JPL # 1 AND NPL)]
FLOAT ALTITUDES ~ 34 KM
OBSERVATIONS DURING AFTERNOON AND SUNSET
CUT-DOWN AND RECOVERIES, OK.

JUNE 20, 1983 : 2 SIMULTANEOUS LAUNCHES, SUCCESSFUL (JPL#1 AND NPL)
FLOAT ALTITUDES ~ 37 KM
OBSERVATIONS DURING AFTERNOON AND SUNSET
FREE-FALL OF JPL#1 GONDOLA, SOON AFTER CUT-DOWN
NPL PAYLOAD DAMAGED ON GROUND (WIND GUST).

DATA INTERCOMPARISONS

- FLORENCE, OCTOBER 1983 : INVENTORY AND PRELIM. INTERCOMPARISON.
- PARIS, MAY 1984 : CONTINUE INTERCOMPARISON; PREPARE ORAL PRESENTATIONS.
- ? , SEPT. 1984 : FINALIZE INTERCOMPARISON; PREPARE PUBLICATIONS.

BALLOONS INTERCOMPARISON CAMPAIGNS

SPECIFIC SUPPORT

- AIRPLANE AND GROUND COORDINATED OBSERVATIONS.
- NSBF LOGISTICS FOR SIMULTANEOUS HEAVY PAYLOADS LAUNCHES, TRACKING, RECOVERIES.
  TLC-TLM OPERATIONS BOTH LOCALLY AND REMOTELY.
- DEDICATED NETWORK FOR COORDINATING TELECOMMANDS (JPL-BALLOON SUPPORT FACILITY).
- WALLOPS - RADAR SUPPORT FOR ACCURATE MULTI-PAYLOADS LOCALIZATIONS.
- PHYSICAL ATMOSPHERE CHARACTERIZATION (P, T) FROM SATELLITES DATA AND RADIO SOUNDINGS (AMES RESEARCH CENTER AND AES).
- INTERCALIBRATION OF PRESSURE SENSORS (NPL AND NSBF).

MAP 2-7

Comparis of Dataset from Balloon Intercomparisons

		HCl	HNO_3	CH_4	NO	NO_2
1.	Liege (PS)	$(2.0 \pm 0.6) \times 10^{14}\ cm^{-2}$ column density above 39 Km		$6.3 \times 10^{16}\ cm^{-2}$ above 39 Km		
	(4 hrs after sunset)	$1.4 \times 10^{15}\ cm^{-2}$ $h > 21.6$ Km		$1.3 \times 10^{18}\ cm^{-2}$ $h > 21.5$ Km		
2.	FRANCE					$1 \pm 0.5 \times 10^{8}\ cm^{-2}$ $h > 30$ Km
3.	NPL, Reddington		$0.4\text{-}15 \times 10^{9}\ cm^{-2}$ at 35 Km			$6 \times 10^{8}\ cm^{-2}$ at 39 Km 10^{9} at 30 Km
4	FRANCE (LOISNARD)	0.56×10^{9} (30)	1.2×10^{9} (30)		0.85×10^{9} (30)	$2.6 \times 10^{9}\ cm^{-3}$ (30)
5.	ROSCOE (UK)				1×10^{9} /km at (30 km)	8×10^{7} (afternoon) 8×10^{8} (night) (43)

MAP 2-16

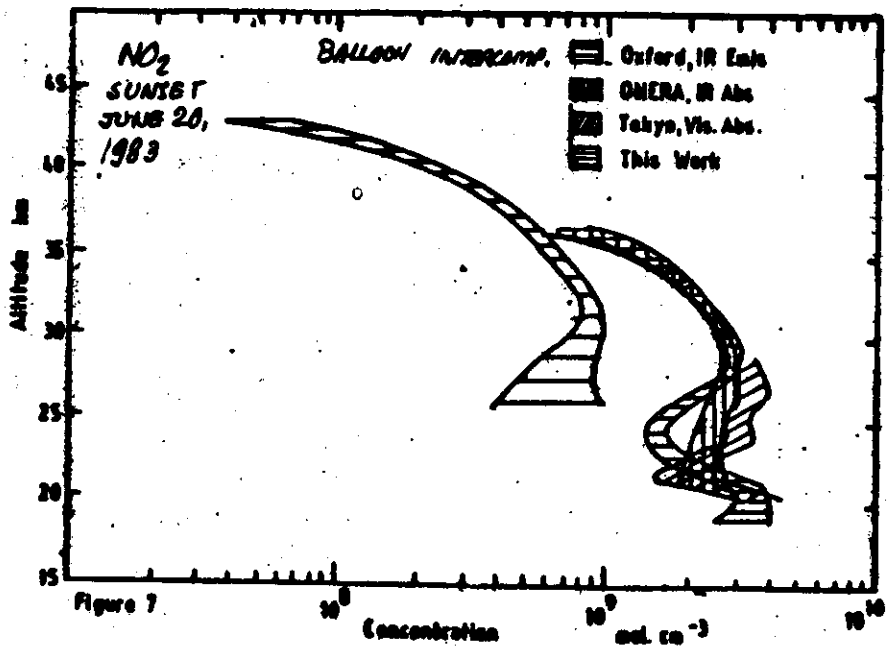

Figure 7

1983/84 STRATALERT

- During every winter STRATALERT BERLIN message prepared daily and circulates via WMO network
- For 1983/84 MAP-WINE Program, preparation of daily STRATALERTS was based on:
  - UK Met office, Bracknell, transmitting daily maps of radiances of NOAA SSU: 10,1 mbar chart
  - European Centre for Medium range Weather Forecasts at Reading, UK, transmitting daily 3- and 5-day forecasts for 30 mbar level
  - University of Colorado, Boulder, provides daily temperatures measured by SME satellite (SOLAR MESOSPHERIC EXPLORER)
  - CNRS, Paris, provides temperatures of middle atmosphere measured by LIDAR at HAUTE PROVENCE
  - University of Saskatchewan, Observatory at Kuhlungsborn (GDR) and Observatory at Collm (GDR) provides information on prevailing winds

Statospheric Research Group at Berlin (FU) analyzed charts upto 10 mbar level, using (i) radiosonde (ii) rocketsonde (iii) SATEM (satellite soundings), and provides forecasts.

MAP WINE

WINTER
1983/84

Austria, Canada,
Czechoslovakia, Denmark,
France, USSR, FRG, GDR,
Norway, Sweden, Switzerland,
UK, USA, USSR

14 sounding vessels
18 Cloff
58 Falling Sphere
49 met aircraft
2 aircraft flights
Hundreds of hours observation
by 4 radars, 5 optical systems

4 lidars with sounding vessels
from Hess Island & Volgograd (USSR)

↑ MAP-1

↑ MAP-DYNAMICS
1982/83 Winter Campaign

From Met Office Bracknell, UK : Daily charts of radiances for NH at Channels 26 and 27 of ESU (Stratospheric Sounding Unit) onboard NOAA Satellite, and 10 daily 1mb height charts from these data

From Clarendon Laboratory, Oxford : Retrieves temp. distr. over NH at 1, 0.3, 0.1 and 0.03 mbar from SAMS (Stratospheric and Mesospheric Sounder onboard Nimbus 7

From Geophys. ob. Collm, GDR : Routinely winds at mesopause alt. over Central Europe from LF drift meas.

From Univ. of Essex, Chelmsford : PR lidar - aerosol/cloud studies

From Sheffield, UK : Ozone with Dobson meter

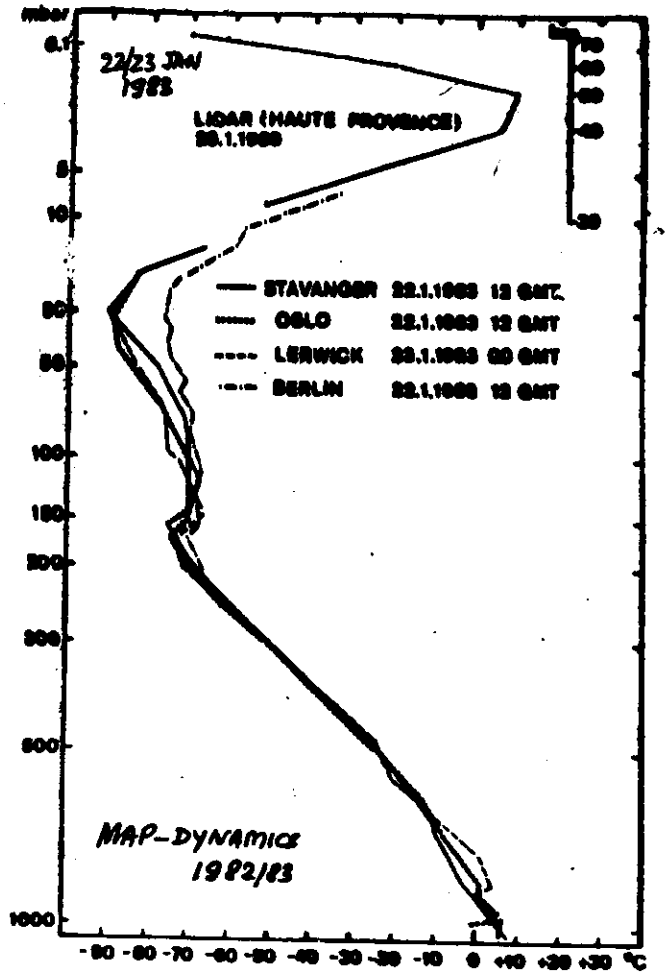

Radiosonde ascents at several stations over Europe on 22/23 January and lidar observation over Haute Provence (courtesy Service d'Aeronomie, Verrières-le-Buisson, France).

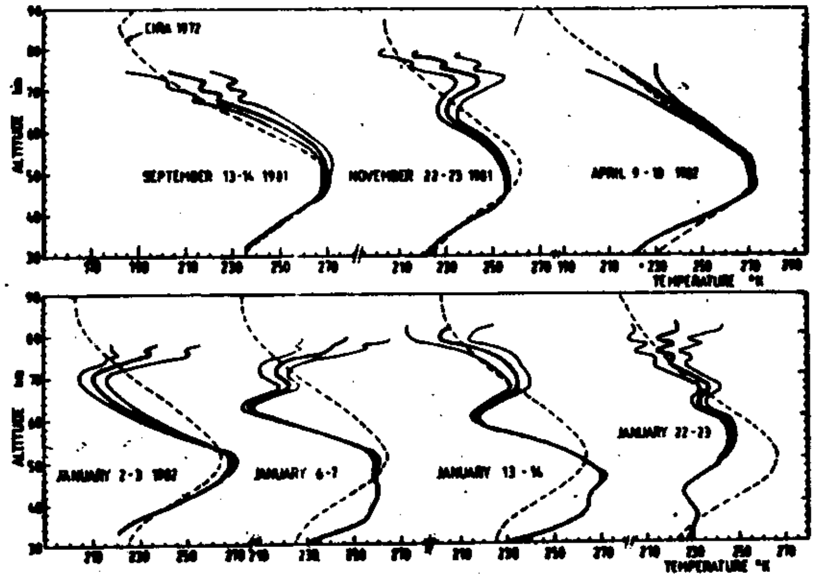

. Series of 7 Lidar temperature profiles obtained from September 1981 to April 1982. The dotted line represents the Cira (1972) model for the corresponding month and latitude. The standard deviation (±σ) is indicated.

MAP 2-14

MAP DYNAMICS 1982/83

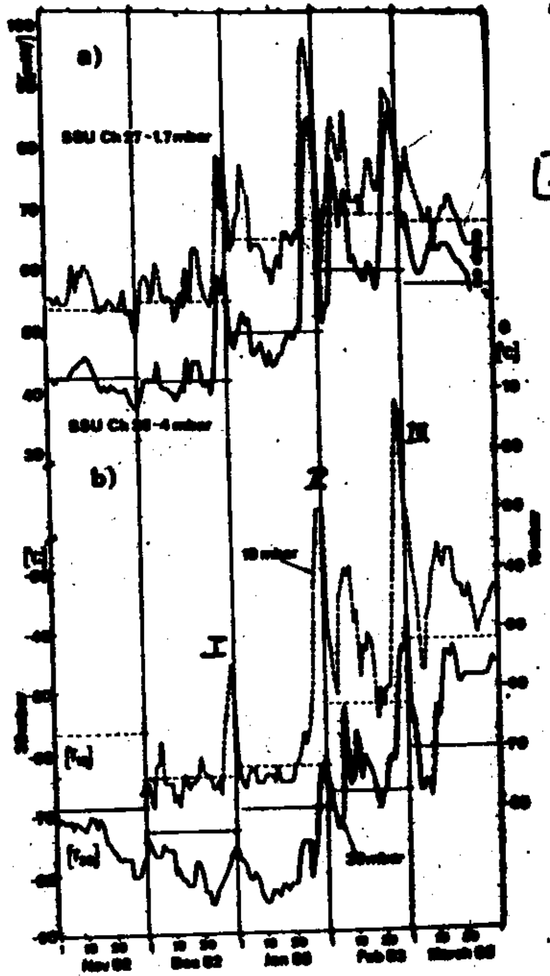

March of radiances and temperatures over the North Pole (horizontal lines are long-term monthly means):

a) Radiances [$mW/m^2sr\ cm^{-1}$] of channel 27 and 26 of the SSU, maximum weight around 1.7 and 4 mbar (courtesy Meteorological Office Bracknell, U.K.).

b) Temperatures [°C] at 10 and 30 mbar (data Free University Berlin).

3 Warming Periods

I Lidar data (Tours) Showed stratopause warming at 45km. Also Heiss Island observation. Short-lived circulation reversal of wind.

II. End of January. Temp. gradient between 60°N and Pole reversed in upper stratosphere down to 10 mb. Similar behaviour in Haute Provence and Heiss Island. However, no breakdown of polar vortex.

III. Third warming at end of February. Warming at middle and lower stratosphere much stronger than before.

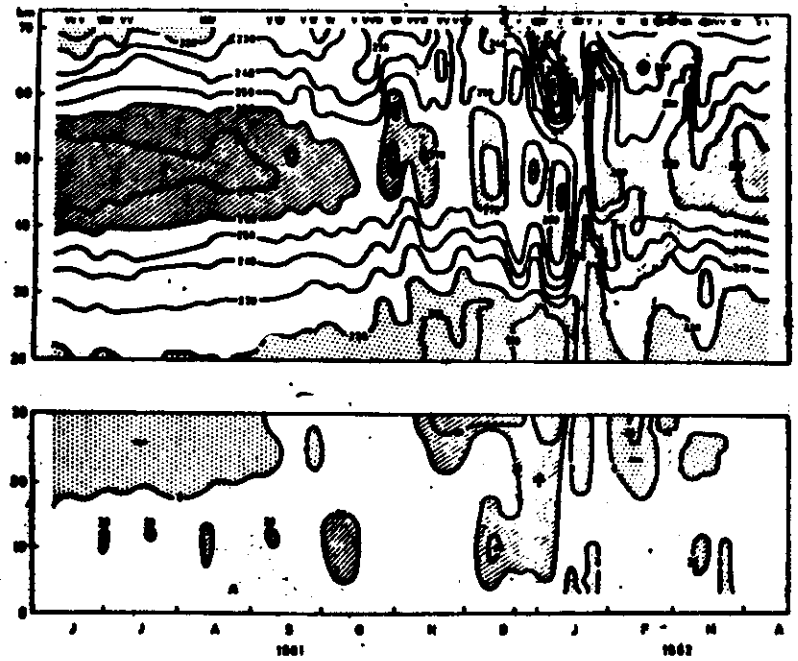

(Top): Time height section of Lidar and radiosonde temperature (K). The contour lines are plotted in steps of 10 K. The arrows above indicate the days when Lidar data were recorded. Shaded areas correspond to temperatures above 260 K, dotted areas to temperatures below 220 K. (Bottom): time height section of the radiosonde zonal wind (m s^{-1}) Westerly winds are >0 and represented by the shaded area; easterly winds are <0 and represented by dotted area. Contour lines are plotted by steps of 20 m s^{-1}.

MAP-PE-IC

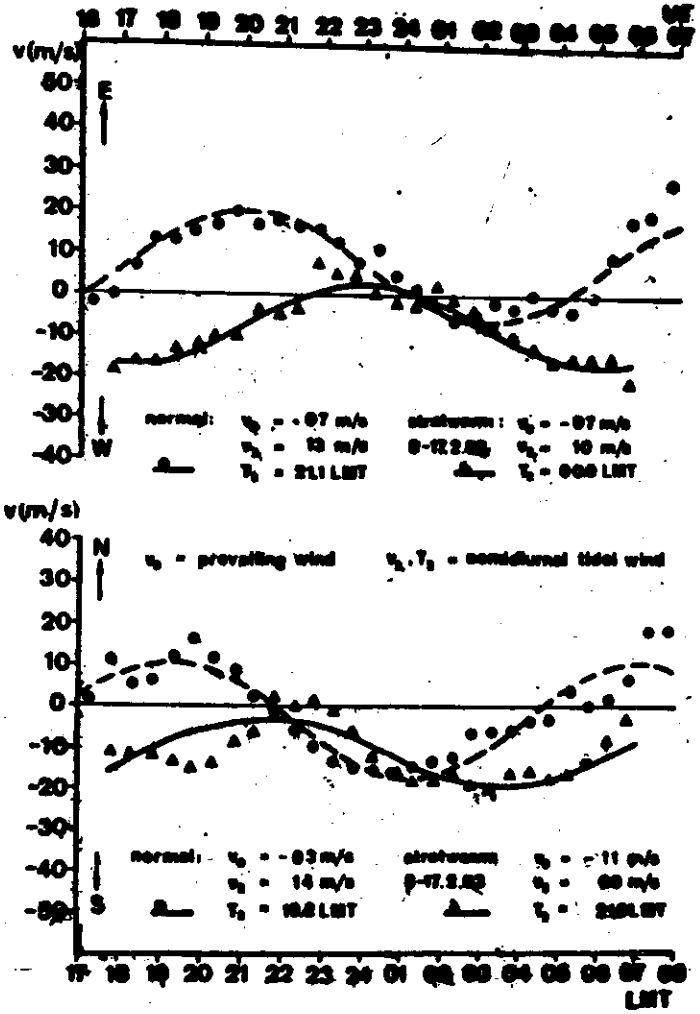

Effect of the Ramagya 1983 stratospheric warming in the upper mesopause wind field (80-85 km) over central Europe obtained from low frequency drift measurements on three sounding paths (129, 237, and 272 kHz).

(contributed by R. Schminder, Geophysical Observatory Collm, GDR)

SIMON

Uncertainties on solar ultraviolet irradiance measurements and fut

	Wavelength intervals (nm)				
	Ly-α	135–175	175–210	210–240	240–400
Accuracy	± 30% ± 10%+	± 30–20% ± 10%+	± 30–20% ± 10+	± 20–10%	± [illegible]
Achieved accuracy on irradiance values	± 30%	± 30%	± 20%	± 15%	± 10%
Discrepancies	200%	100%	40%	20%	20%
Uncertainties on spectral irradiance transfer source standards	± 3%*	± 10% ± 3%*	± 6% ± 3%*	± 5% ± 3%*	[illegible]
27-d variability	100–30%	12%	10–4%	2%	2–[illegible]%
11-yr variability	100%	< 120%	< 20%	< 10%§	< 5%§
Goals: accuracy	± 10%	± 5%	± 5%	± 5%	
Goals: precision	± 5%	± 5%	± 2%	± 1%	

+ at 2σ level, using the SURF as calibration standard

* Synchrotron Users Radiation Facility (SURF), at 2σ level

§ according to model calculations published by LEAN ET AL. (1982).

49

RMP 2.47

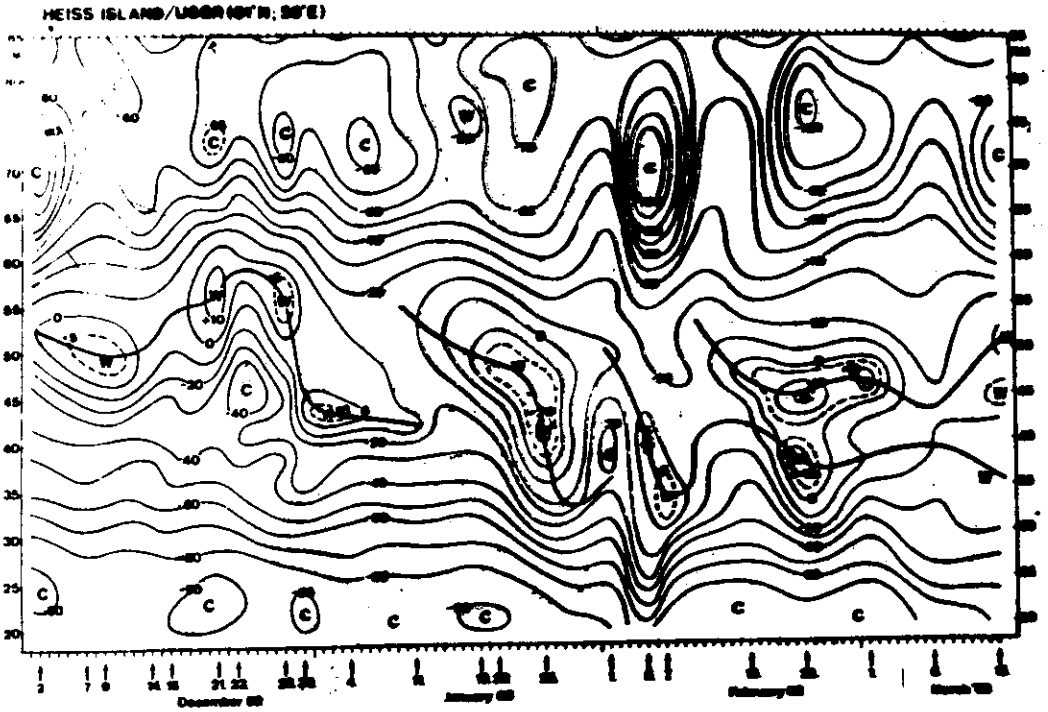

Time height section of rocketsonde temperatures [°C] from 2 December 1982 to 15 March 1983.

48

HERZBERG CONTINUM

$O_2 \xrightarrow{2000\text{-}2420\,A} O + O$
(major source of atomic oxygen below 60-65 km).

Extends from 2424 Å to appr. 1500 Å. with max. cross section ~ 1×10^{-23} cm^2 bet. 1950 - 2000 Å.

At $\lambda <$ 2000-2100 Å, lies beneath Schumann - Runge bands and makes a minor contribution to total absorption.

SO: Herzberg continuum usually is referred to over 2000 - 2420 nm Å (strictly speaking incorrect).

Lab. absorption cross sections by DITCHBURN & YOUNG, BLAKE ET AL., SHARDANAND, OGAWA, & HASSON - NICHOLLS (1971), SHARDANAND AND PRASAD RAO (1977.

VALUES (extrapolated to zero pressure) range over a factor of at least 2, possibly due to inadequate pressure correction.
New work with balloonborne spectrometers inferring cross section from attenuation of solar radiation after correction of atmospheric opacity caused by O_3. (Frederick and Mentall, 1982, Herman and Mentall, 1982).

Recommendation: Solid curve in diagram
Group feels best selection from existing lab data are of OGAWA (1971) for $\lambda \leq$ 2200 Å with those for $\lambda <$ 2050 Å corrected for band contribution

Impact: Expect valuable contribution to quantitative estimates of solar energy deposition in the middle atmosphere.

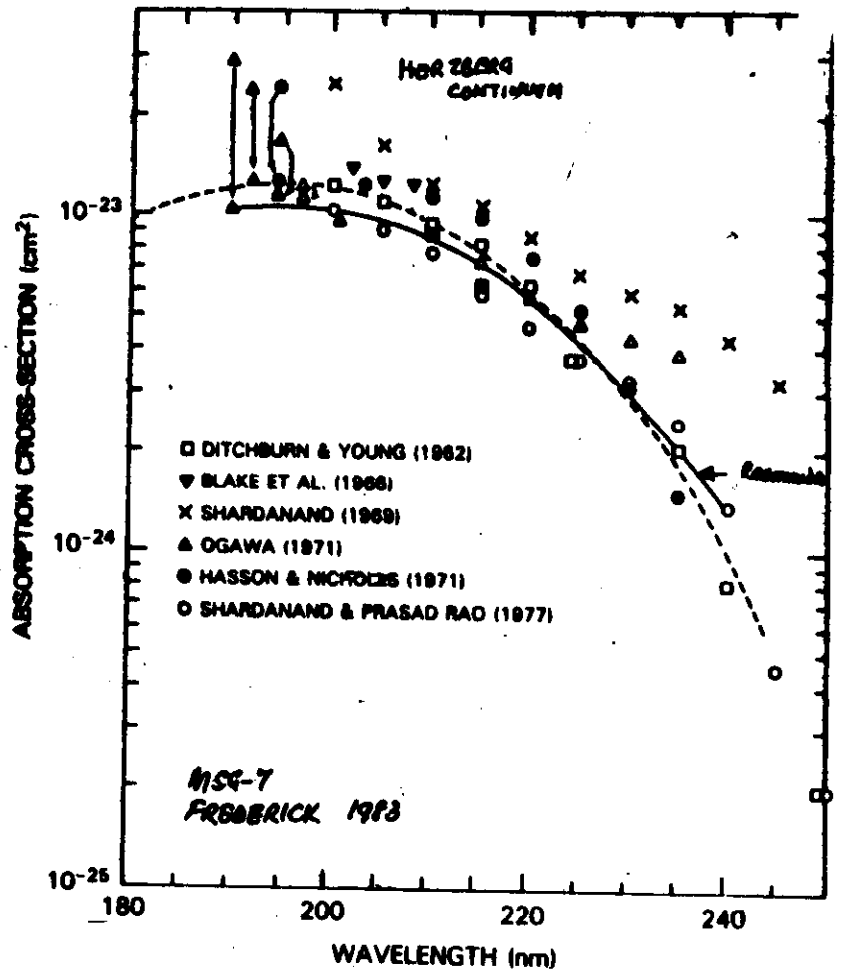

Laboratory measurements of the Herzberg continuum absorption cross section of molecular oxygen. The dashed line indicates theoretical results of Jarmain and Nicholls (1967). The solid line defines the recommended values.

SCHUMAN-RUNGE CONTINUUM

Range : 1250-1300 Å to 1750 Å.

Interf : For $\lambda < 1650$ absorption at Alt ≥ 100 Km
$\lambda > 1650$ For trioste atmosphere

Remarks: For $\lambda > 175$ nm cross section composed of closely spaced absorption lines belonging to Schumann-Runge band system with the underlying Schumann-Runge continuum.

Inclusion of absorption by S-R bands poses formidable problems because of rapid variation of cross section with wavelength. Nevertheless, critical for calculation of resolution $q(0)$.

Predissoc. of O_2 by S-R bands → major source of O bet. 60-95 Km

Diss. by Hartley cont $\lambda > 2000$ Å → lower altitude

Diss. of N_2O and CFMs

Lα

Lewis et al (1981) Spectral resolution of 0.005 nm req.

Table in MAP Handbook 8 : 121.46 to 121.70 nm at intervals of 0.2 nm.

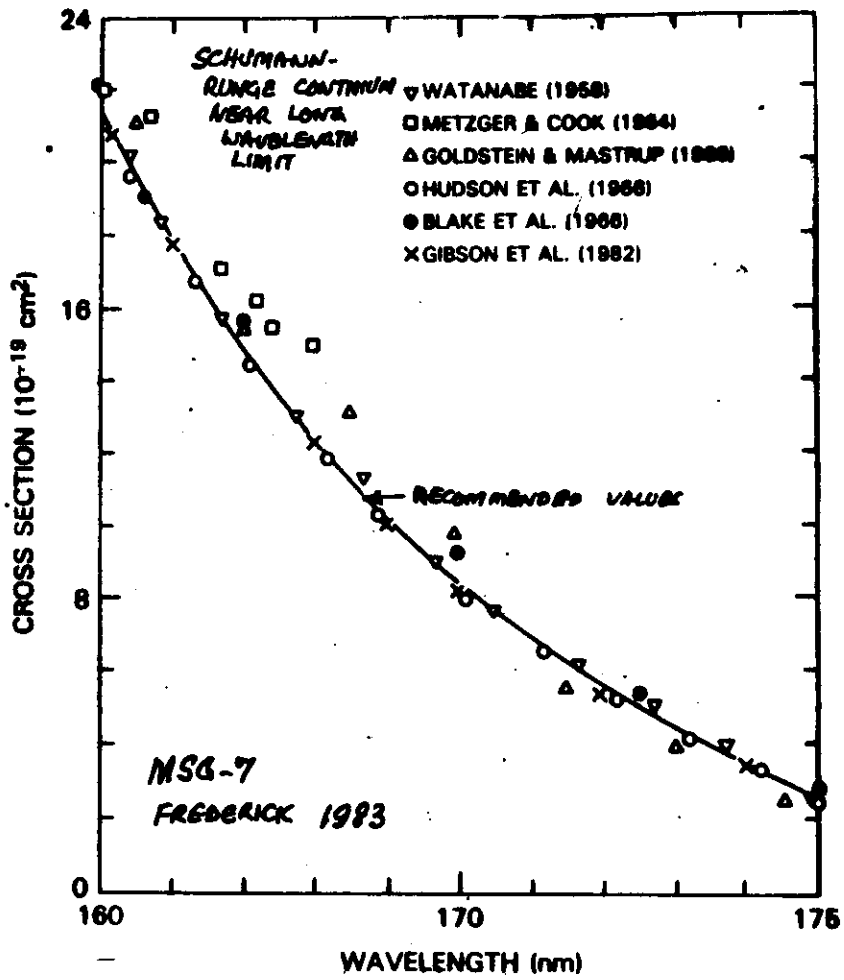

Laboratory measurements of the Schumann-Runge continuum cross section near the long wavelength limit. The solid line defines the recommended values.

Observations and chemistry

A. P. MITRA
National Physical Laboratory of India
New Delhi, India

Abstract. — We describe in this article the observations and chemistry of the ionisation of the Earth's Middle Atmosphere, here defined as the region between 100 km and the Tropopause, consisting of the D-region (50-100 km) and the ionisation in the Stratosphere. In this, atmospheric trace constituents play a dominant role and chemical reactions, both neutral and ionic, are dominant. Observational data on electron and ion distributions and on ion composition, both for the D-region and the Stratosphere (for the latter more limited), are discussed. Chemical schemes, which were until recently confined to conditions in the D-region, have now been extended to stratospheric heights; some of these schemes are also outlined.

1. INTRODUCTION

The Earth's Middle Atmosphere is a relatively small part of the earth's total environment but it provides a link between the lower and upper atmospheres. The region we are concerned with covers all levels below 100 km, thus including the D-region and the Stratosphere. The definition of the D-region is somewhat arbitrary. The most common definition is the region of ionisation extending from 50-100 km including the mesopause around 85 km where the atmosphere reaches its lowest temperature of about 140-170°K. Under normal conditions, the electron density vanishes at and below 60 km, but at times of solar disturbances appreciable electron concentrations are observed down to 40 km.

Below the lower boundary of the D-region, ionisation does not completely vanish although electrons disappear. Ions in appreciable number continue down to tropospheric heights. The separation between the Stratosphere and the Mesosphere is, therefore, artificial, and the entire region from tropopause to turbopause — roughly between 15-110 km — should be considered as one region. We do so in this article.

The practical applications of such studies are numerous. The primary ones on which work has been done in the past, involve HF shore-to-shore and ship-to-ship communication, aircraft communication especially on trans-polar flight paths, long range navigation, time and frequency transmission and, effects of disturbances (both manmade and natural). In all these areas, current requirements and future needs call for improved understanding of the D-region

54

and for a continuing need for the construction of D-region models, especially for problems that require ray-tracing of the radio wave path. Another new application appears to be the concept of atmospheric global electrical circuit providing a mechanism of coupling for sun-weather relationship. For the Stratosphere, the question of ozone depletion by manmade vis-a-vis natural inputs has assumed major significance. The possible role of ions in these changes has not been considered adequately. Nevertheless, such effects are possible, especially at times of solar disturbances.

2. The D-region

2.1. *D-region Electron Density*

Purely from the view point of its extent, the D-region constitutes a very small part of the total ionosphere: it extends over some 50 km only (from 50 to 100 km), and has maximum electron density (N_e) during day of about 10^3 cm^{-3} at 85 km, about 1/100th of the peak density in the E-region and about 1/500th to 1/1000th of the F-region electron density. What makes this narrow and weak plasma region significant is its location and the interplay of the minor constituents.

The lower ionosphere electron density profile can be classified into four distinct regions (Rowe et al., 1974) (see Fig. 1 and Fig. 2).

(1) A region about 85 km — the simplest part of the D-region.
(2) A region where electron density increases rapidly — the so called 'Ledge' region around 82-85 km.
(3) A region between the ledge and 70 km.
(4) The region below 70 km where negative ions begin to become appreciable — the 'negative ion region'.

In Region 1 the ions are primarily molecular, consisting of NO^+ and O_2^+. Recombinations of these ions are straightforward and involve the following dissociative recombination processes:

$$O_2^+ + e \rightarrow O + O \qquad 2\times10^{-7}\left(\frac{300}{T}\right)$$

$$NO^+ + e \rightarrow N + O \qquad 4\times10^{-7}\left(\frac{300}{T}\right)$$

This is the simplest region and one for which at the present time prediction is the most accurate.

In Region 2 the electron density increases by almost an order of magnitude within a few kilometres. This sharp 'ledge' in N_e occurs around 82-85 km and is observed in most rocket flights during the day, except at sunrise and sunset.

In Region 3 the electron density is nearly constant (a few hundred per cubic cm), and the most dominant characteristic is the existence of a whole series of water-cluster ions $H^+(H_2O)_n$.

Region 4 covers all levels below 70 km where negative ions emerge as an important, and eventually dominant, parameter.

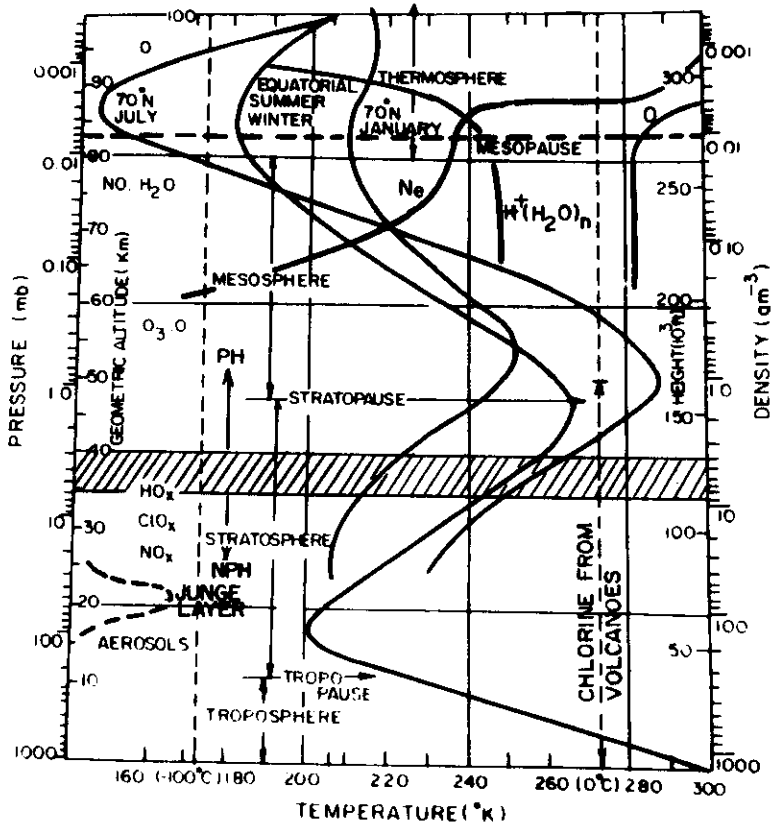

FIG. 1. The atmosphere below 100 km, including the boundaries of the Troposphere, Stratosphere and Mesosphere, as well as two special levels — one around 85 km and the other around 35-40 km. At the 85 km level, there are sharp changes in many parameters including temperature, atomic oxygen concentration, electron density and positive ion clusters. At the 35-40 km level, ions change over from proton hydrates to non-proton hydrates.

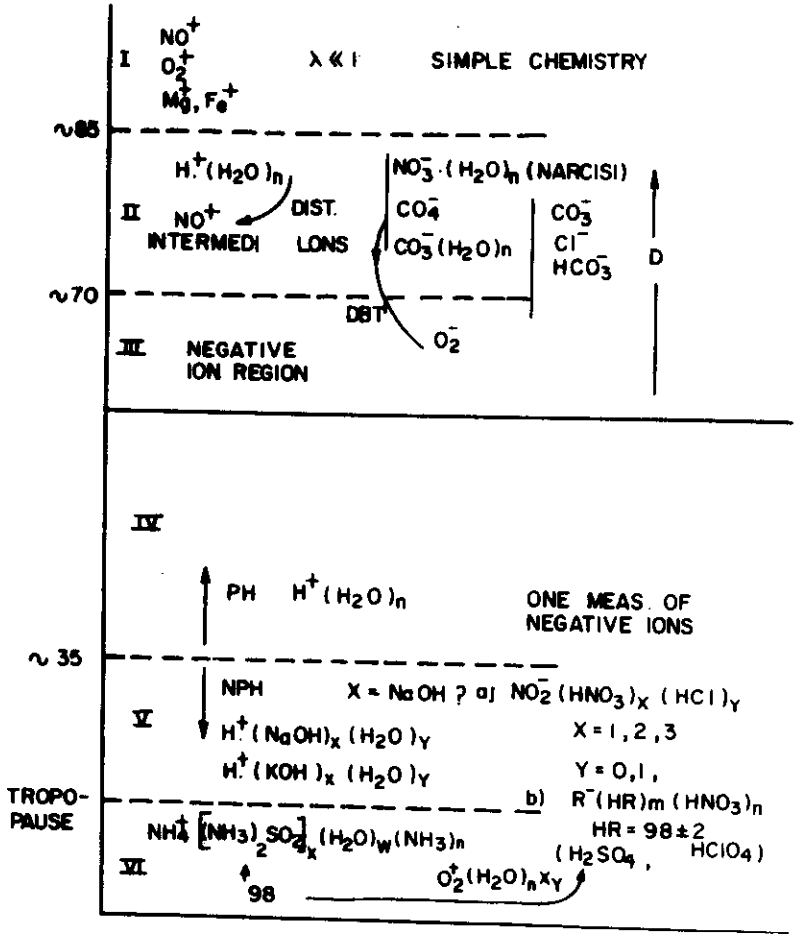

FIG. 2. A classification of the middle ionosphere in terms of ions. Six sub-regions can be identified.

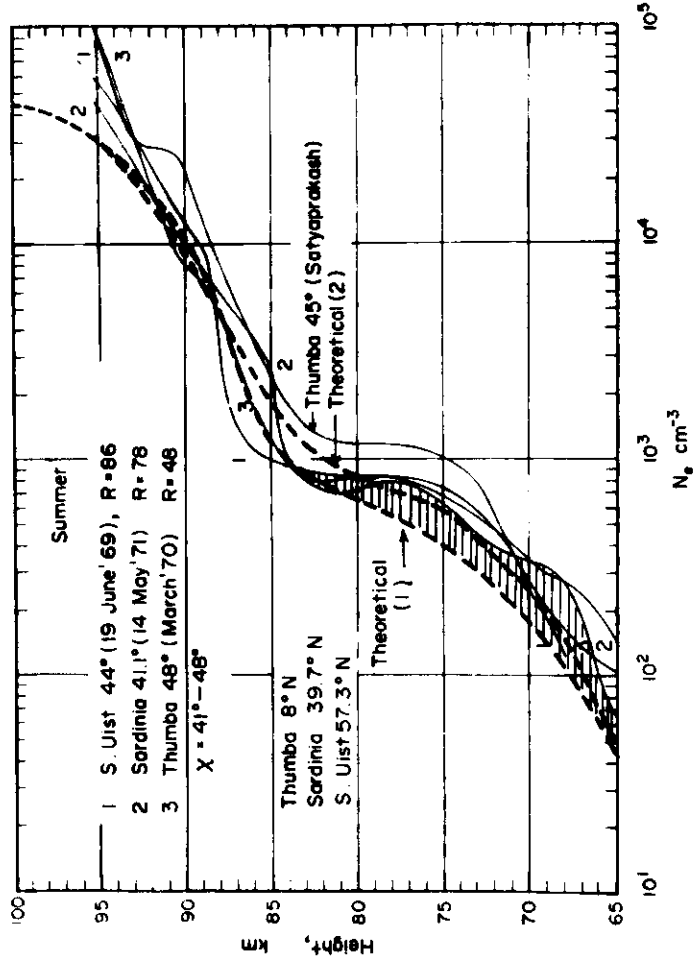

FIG. 3. N_e profiles for three widely different locations: Thumba in India (8°N, an equatorial station), Sardenia in Spain (39.7°N, a mid-latitude station) and South Uist in Scotland (57.3°N, a high latitude station). The comparison is made for nearly identical solar zenith angles and moderate solar activity conditions. The main point to note is the close agreement between these profiles for such widely different locations.

For many purposes, including ray-tracing of the radiowave path through the lower ionosphere, one needs to have a description of the complete N_e profile, including its variations with latitude and solar activity. The techniques that have been found very useful in providing reliable electron density values for the D-region have been introduced more recently. These include: (a) the partial reflection technique, in which use is made of the partial reflection from irregularities in the D-region of a high frequency radiowave transmitted vertically: (b) the wave interaction technique, in which the exploring radiowave is modulated in the D-region by another radiowave of a powerful transmitter; (c) the incoherent scatter technique, which makes use of the scattering of radiowaves from the random thermal fluctuations in electron density existing in the plasma, and (d) most importantly, from the use of rockets. The rockets have provided by far the largest information on D-region ionization, and carry payloads which either measure the absorption or polarization characteristics of radiowaves transmitted from the ground or specially designed probes, the most important being the Langmuir probe.

These techniques have been most extensively used only for midlatitudes. Representative midlatitude profiles can be drawn from the many rocket measurements made at Wallops Island and New Mexico in the USA, Sardinia, in Italy, the Woomera range in Australia. They can be drawn also from the crossmodulation experiments in Pennsylvania State University in the USA; partial reflection measurements at Illinois; and Incoherent Scatter facility at Arecibo, Puerto Rico. For the other regions, the most important data have come from rockets flights made at Thumba in the southern tip of India, located almost on the magnetic equator, and from South Uist in Scotland, Ft. Churchill in Canada, and Kiruna in Sweden, all located in high latitudes, as also is the IS facility at Chatanika, Alaska. When these different N_e measurements are compared one finds that the profiles are essentially identical in summer for all places in the world (excepting perhaps at the levels of the ledge) for the same conditions of solar activity and for comparable solar zenith angles. An example of this kind, shown in figure 3 gives a comparison for Thumba (8°N), Sardinia (40°N), and South Uist (57°N). In winter, however, the high latitude N_e profiles present a different picture, being highly variable from one day to anohter. On certain days N_e is greatly enhanced (these are the days of high absorption — the so-called winter anomaly). Further, because it is directly exposed to solar particle streams, it is more sensitive to such disturbances.

The sharp rise in electron density around 82 km is one of the most distinctive features of the D-region. Interestingly, this level also coincides with the height at which there is sudden change in the positive ion composition, with water cluster ions (see below) replaced by NO^+ and O_2^+. This sudden rise in electron density comes not from a change in the solar radiation but from the sudden decrease in the rate of loss of electrons with the ions as a consequence of the change in the ion composition.

·59

2.2. *Positive and negative ions in the D-region*

An entirely unexpected result is the existence of a large quantity of water cluster ions in the D-region. These take the form of $H^+(H_2O)_n$ with $n = 1-7$. They are dominant only in the lower part of the D-region, and the upper part shows a drastic drop at precisely the heights around which we observe the ionization ledge (figure 4). Above these heights the ions are principally NO^+ and O_2^+, with an admixture of CO_2 and N_2 cluster of NO^+ and O_2^+. Further up, near 93 km, there is a broad layer of metal ions, principally Fe^+ and Mg^+, believed to be of meteoric origin.

The water cluster ions were initially considered to be contaminants. The origin and behaviour of these ions have formed the basis of the most serious work in D-region chemistry during the last decade. Although the existence of these ions is now beyond question, there is doubt about the relative proportion of H_3O^+, $H_5O_2^+$, $H_7O_3^+$ ... ions, since fragmentation of complex weakly-bound ions can occur. Higher order ions have been observed when the mesosphere is cold, as in high latitudes in summer or with low velocity rockets, or during the downleg of a rocket trajectory when the shock conditions are reduced. Since the exact proportion of different orders of water cluster ions is in doubt, the current practice is to take the sum $\Sigma H^+(H_2O)_n$ and express this as a ratio of the precursor ions NO^+ and O_2^+ in the form:

$$f^+ = \frac{H^+(H_2O)_n}{NO^+ + O_2^+}$$

The parameter f^+ and the level Z_o at which the cluster ions rapidly disappear are two very crucial parameters for the D-region.

A very strange feature of the D-region is that while it is so complex during normal times, it becomes much simpler (complex ions disapear and simple molecular ions dominate) during disturbed times when increased solar XUV radiation (as in flares) or particles (as during Polar Cap Absorption Events, PCA's) impinge on the atmosphere or when, as sometimes happens in high latitudes in winter, there is a period of mesospheric warming. Indeed, these seem to be the only times when the D-region ion composition simplifies to a combination of the molecular ions NO^+ and O_2^+ (Fig. 1 & 4), down to about 70 km. Below 70 km, however, the cluster ions continue to dominate. The net result is as if the level Z_o has moved downwards during these disturbed times. The second feature that distinguishes the D-region from the higher layers is the existence of negative ions. The ratio

$$\lambda = \frac{N^-}{N_e}$$

is a characteristic parameter of the D-region chemistry in the same way as f^+ is for positive ions below Z_o. The two parameters f^+ and λ act like two important sensors for the D-region chemistry.

60

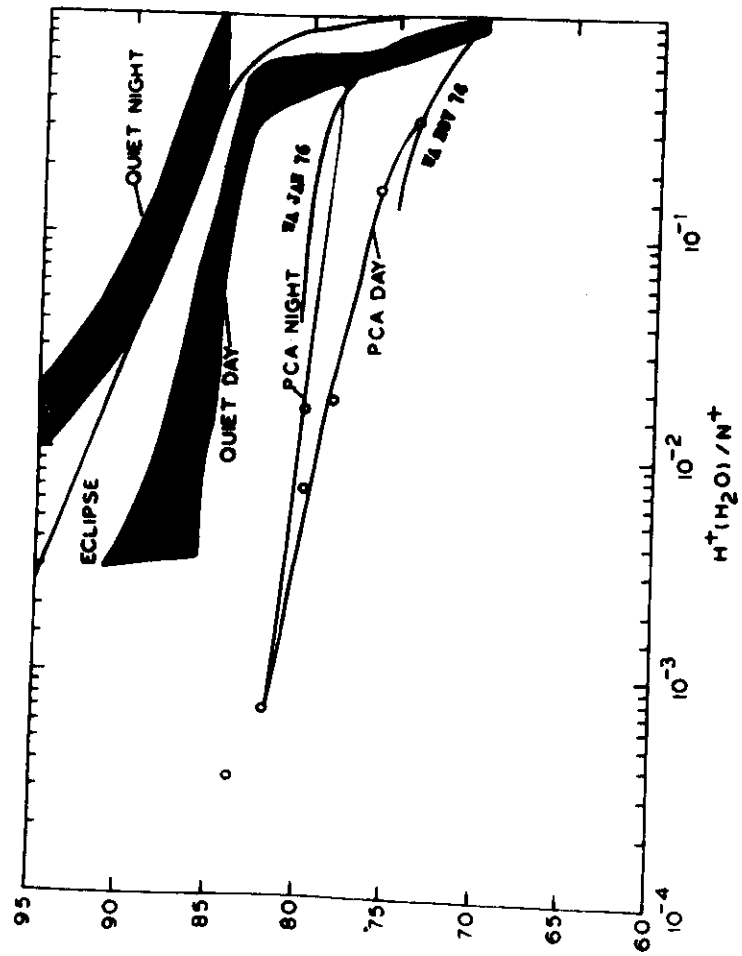

Fig. 4. Variation of hydrated ion component as a function of height. Note the sudden decrease in the cluster concentration at specific heights which are different for different conditions.

The primary negative ions are O^- and O_2^-. However, as in the case of positive ions, mass spectrometric measurements show the existence of a wide variety of negative ions which cannot be the result of direct attachment. The dominant series identified by one group was $(NO_3^-)(H_2O)_n$ with a possible admixture of $(CO_3^-)(H_2O)_n$, with $n=0$ to 5. The results of the second group showed that CO_3^- was the major ion below 80 km, with HCO_3^- and Cl^- and NO_3^- also present.

2.3. *The disturbed D-region*

There are two major kinds of disturbances in the D-region: one of solar origin, the other due to local dynamic or thermal changes. In the first category, we have the effects of solar flares and PCA's. In the second category, the most important effect is the so-called winter anomaly and mesospheric warming or cooling events that occur in winter at latitudes above 35°. In both cases, there are profound changes not only in the ionization of the D-region but in the nature of positive and negative ion composition as well.

For both solar flare events and PCA's the primary and fundamental effect is one of increased ionization in the D-region. The actual magnitude of enhancement depends on the severity of the effect. Some illustrative examples are shown in figure 5. For a very large solar flare, or a large PCA event, N_e at 80 km may increase from $10^3\,cm^{-3}$ to $10^4\,cm^{-3}$, and the D-region will extend well below its normal cut off at 60 km, to perhaps around 40 km. These large ionizations in the lower D-region at heights of high collision frequency are responsible for complete blackouts of HF and medium-wave communications; they must, therefore, be anticipated and alternative channels of communication planned. The increase in ionization is not the only effect observed. Apart from a drastic reduction in water ion cluster percentage and emergence of NO^+ ions as the principal positive ions above 70 km, there are probably changes in some of the neutral minor constituents. Nitric oxide is believed to be enhanced during a PCA perhaps by as much as a factor of ten; ozone concentration is decreased; and atomic oxygen concentration increased.

We have so far discussed only disturbances of solar origin. Amongst those of local (or atmospheric) origin the most important is the event known as the Winter Anomaly. At latitudes above 35° there are days when HF absorption is found to be very large indicating that on these days either the electron density or collision frequency is increased. Several rocket flights undertaken during such anomalously high absorption days have shown that is N_e that is enhanced; this increase in N_e extends essentially throughout the D-region down to at least 70 km (Fig. 6). It is believed that this change is a result of accumulation of NO, which is built up by vertical transport of atomic species downwards from the turbopause region.

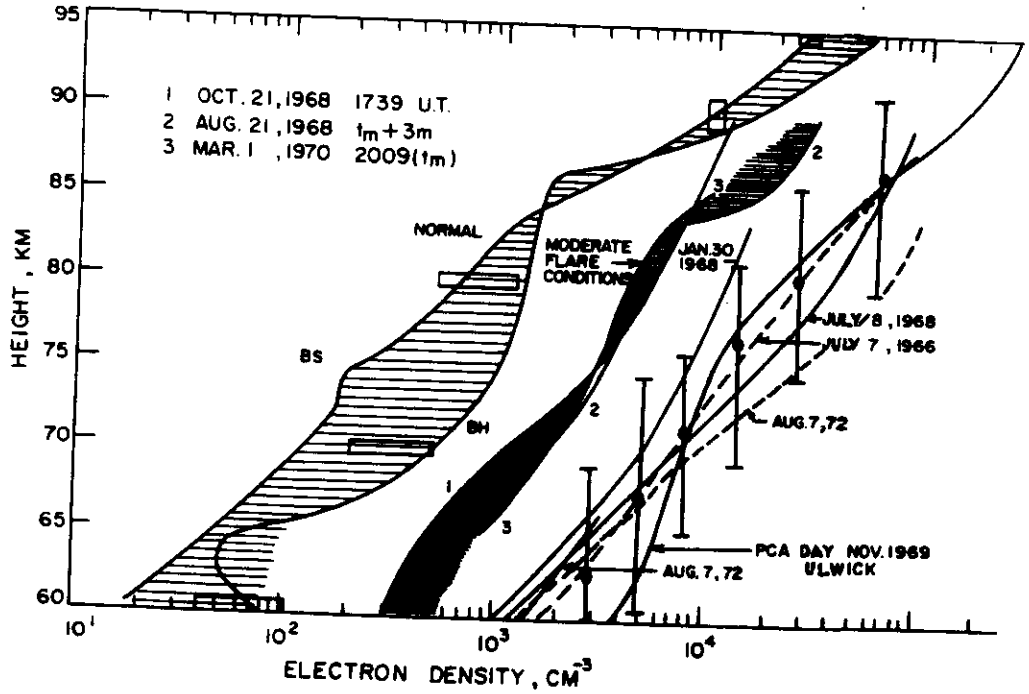

FIG. 5. N_e profiles under normal as well as disturbed conditions of solar disturbances. The disturbances include direct solar flare effects due to PCAs.

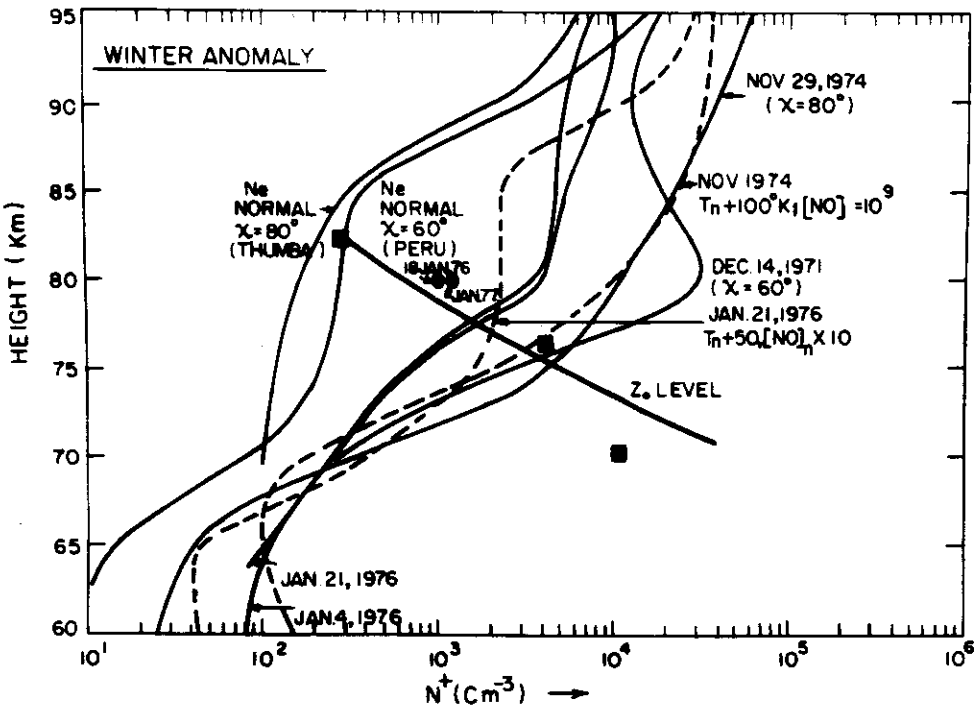

FIG. 6. Changes in ionisation in the D-region during winter anomaly. The events included are those of December 14, 1971, November 29, 1974 and January 1976. We also show (the solid thick line) the fall in Zo level during winter anomaly.

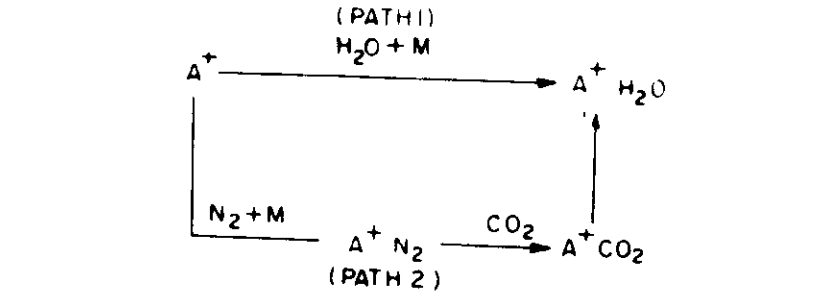

(a)

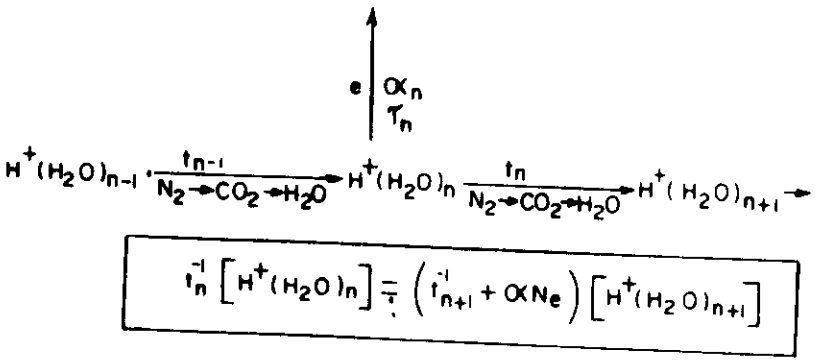

(b)

FIG. 7. The scheme outlined in (a) gives two possible paths in hydration of the precursor ion A^+. Path two is apparently preferred for low mesospheric temperatures. The bottom scheme (b) compares the hydration time with recombination time.

2.4. *The chemistry of the D-region*

Of the solar radiation incident on the atmosphere, only the following wavelengths can penetrate below 100 km:

(1) Shortwavelength X-rays.
(2) The series of windows in the range 1100-1300 Å, including L_α.
(3) Wavelengths above 1900 Å.

Under normal conditions, the main ionization source below 65 km is galactic cosmic rays; that below 85 km is principally photoionization of NO by L_α in one of the windows in (2); and above 85 km it is X-rays in the wavelengths up to 100 Å and ultraviolet radiations in wavelengths less than 1030 Å. The first and the third processes produce initially N_2^+ and O_2^+ ions, and the second process NO^+ ions. The initial or the precursor ions are therefore, N_2^+ and O_2^+ below 65 km; NO^+ ions between 70-85 km and NO^+, O_2^+, N_2^+, and O^+ ions between the 85-100 km.

The ions, however, do not remain in this form. The first casualties are the N_2^+ ions, which are immediately converted into O_2^+ ions through the reaction

$$N_2^+ + O_2 \rightarrow N_2 + O_2^+$$

which is very fast so that for D-region heights the lifetime of the N_2^+ ion is in the range of a nanosecond to a millisecond. The principal question is how these O_2^+ and NO^+ ions get converted into the cluster ions $H^+(H_2O)_n$. At heights where O_2^+ ions dominate (below 65 km, for instance), the sequence of conversion is clear.

The most crucial chain is the following:

$$NO^+ \xrightarrow{k_1} NO^+N_2 \xrightarrow[CO_2]{k_2} NO^+CO_2 \xrightarrow[H_2O]{k_3} NO^+H_2O$$

R. Johnsen et al. (1975) have reported, from laboratory measurements, that the forward reaction $NO^+ \rightarrow NO^+N_2$ is sufficiently fast with $k_1 = 2.0 \times 10^{-31} \left(\frac{300}{T}\right)^{4.4}$. At mesospheric temperature (say 200°K) $k_1 = 2 \times 10^{-30}$ so that at 80 km, the characteristic time of this reaction is only 4 seconds, well within the required criterion. Of the two possible paths indicated in Fig. 7a, path 2 is preferred for low mesospheric temperatures.

Two most significant parameters in the D-region chemistry are respectively nitric oxide concentration and atmospheric temperature. The role of the former was recognized for many years and for a long time measurement of nitric oxide in the mesosphere was a major target. On this, observational data for quiet conditions are now adequate — measurements include those with γ-band photometers carried in rockets and in satellites and a number of ionospheric estimates. The NO profile has been shown to be the same, within 25 per cent, in low midlatitudes, although highly variable in polar latitudes; the range within which the NO profile lies at heights between 70-100 km, can

perhaps be set within a factor of 3. The role played by atmospheric temperature is equally crucial, but is still inadequately understood. An increase in temperature has at least two effects: it increases the process of decomposition of higher order clusters to lower orders and inhibits the process of clustering from NO^+. Both decrease the effective recombination coefficient and, therefore, increase the electron density.

For the negative ions, the sequence is believed to be first an attachment of electrons to O and O_2 to form O^- and O_2^-, which then proceed down the electrochemical series in the order of increasing electron affinity until stable negative ions such as NO_3^- and $X^-(H_2O)_n$ are formed. These are lost mainly through mutual neutralization with positive ions, for which the rate coefficient is large (10^{-6}-10^{-7} cm^3/s). At intermediate steps the main processes of loss of negative ions are through detachment which may occur from solar radiations of appropriate wavelengths (photo-detachment) or by collisions with the neutral constituents of the atmosphere (collisional detachment).

In recent years there has been some attempt to arrive at one unified reaction scheme governing the D-region conditions for quiet and disturbed conditions of every sort. In this, two approaches have been made: one includes all known positive and negative ion reactions; the other simplified these in a semi-empirical form in which the more doubtful reactions are lumped together into a parameter whose value is set againts observational data.

Several such simplified schemes exist. The one that has found the widest use is the six-ion scheme of A. P. Mitra and J. N. Rowe shown in Fig. 8. In this, two major simplifications are made, as follows:

(1) Since the relative concentrations of the different orders of cluster ions are not well-determined different orders of $H^+(H_2O)_n$ are lumped together as $\Sigma H^+(H_2O)_n$. From this total sum, the relative concentrations can be separately determined.

(2) The main simplifications concern the hydration of NO^+ to cluster ions. Without actually identifying the processes, the total rate of conversion is given by a parameter B in a channel $NO^+ \xrightarrow{B} H^+(H_2O)$, which can be estimated merely from the observed ratio of $[\Sigma H^+(H_2O)_n]/[NO^+]$. The requirements of B to ensure that water cluster ions form a concentration of 50 per cent of the total positive ions at 80 km is $B \sim 10^{-2}\ s^{-1}$.

This six-ion scheme has allowed the formulation of a unified picture for the D-region; the same picture provides an interpretation of a wide variety of D-region conditions including Polar Cap Absorption Events, Solar Eclipses, Solar Flares, and conditions during quiet days and nights. Even this simple picture gives a remarkably good account of the changes in cluster percentage, as we see in figure 9 given by Mitra. In this, cluster ion percentage is shown as a function of $q(O_2^+)$ for different fixed levels, and typical conditions of night, solar eclipses, PCA's and flares of different degrees are indicated. The most

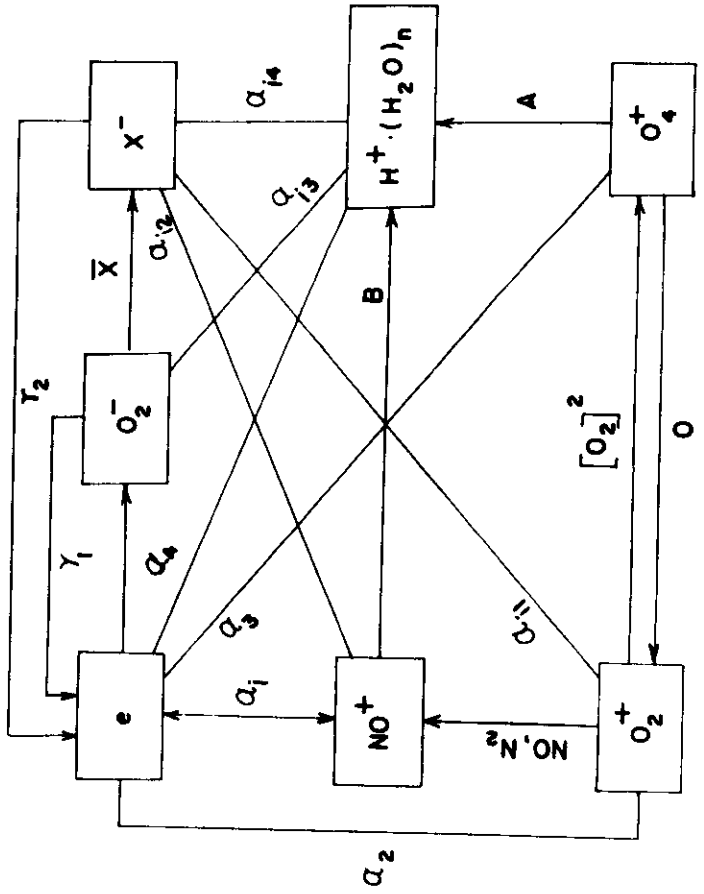

FIG. 8. The six-ion scheme of Rowe and Mitra which combines reactions between electrons and different positive and negative ions in a simplified way. The value of B is obtained directly from observed ratio of $[H^+(H_2O)_n]/[NO^+]$.

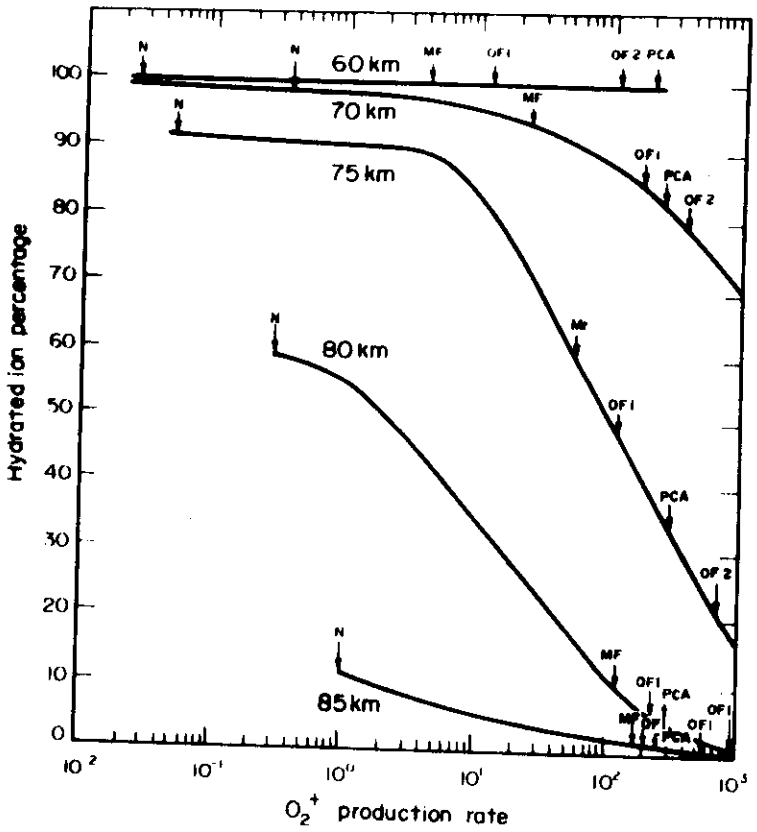

FIG. 9. A «unified» D-region picture — a consequence of the six-ion scheme of Mitra and Rowe (Fig. 8 above). As O_2 production rate is increased (whatever the source), hydrated ion percentage decreases until it reaches a stable minimum value. Capital N represents «normal» conditions; MF - moderate flare; OF - outstanding flare. In this single picture, all conditions can be portrayed.

remarkable consequence is the change in ion composition as $q(O_2^+)$ is changed. At 80 km, the hydrated ion percentage reduces from a value of 50 per cent under normal conditions to only about 5 per cent of the total for a very large solar flare. This reduces the effective recombination coefficient by a factor of 5. We also note that for large values of q, the percentage of hydrates and consequently the value of the effective recombination coefficient level off. Under these conditions the positive ion chemistry reduces to the situación of simple molecular ion chemistry.

In addition, we now believe that (a) an increase in nitric oxide occurs during PCA's and (b) during a winter anomaly there are increases in nitric oxide as well as a change in atmospheric temperature. Furthermore, in recent years attempts have been made in Boulder and Arecibo in the USA, and in at least one location in the USSR, to modify the ionosphere artificially by heating. In such cases the D-region electron temperature is considered to be enhanced from about 200°K to about 1000°K at 80 km, and consequently all reactions in which electrons participate are affected. The consequences of this experiment in electron temperature are an increase in N_e above 65 km, and a decrease in N_e below 65 km (Tomko et al., 1980). The calculated changes as a function of (T_e/T_n) are shown in Fig. 10.

3. Stratospheric ionization

3.1. *Stratospheric Positive Ions*

In the stratosphere electrons are virtually non-existent, but positive and negative ions are appreciable. Measurement of these ions and stratosphere have been made for many years. Ion concentration seems to be between 10^2 and 10^3 cm^{-3} at stratospheric heights progressively increasing from low to high latitudes. In some measurements, there are pronounced holes in ion distributions that, we shall see later, may arise due to recombination of ions with aerosols.

To understand, however, the basic characteristics of the ion chemistry at stratospheric and tropospheric heights, we should have information on ion composition. There are profound changes in ion composition as we go down from the mesosphere to stratosphere (Fig. 2). The first such information came from rocket measurements by Arnold et al. (1978) in Germany; there were three such measurements. The most important result in these flights was a changeover ion PH (Proton hydrate) dominance to NPH (Non-proton hydrate) dominance at about 35-40 km. Since there was a possibility that in the rocket measurements the higher order of cluster ions are dissociated, balloon measurements have been undertaken more recently. Three sets of balloon measurements have been made recently one set by Arnold et al. (1978) (three daytime flights over south West France on September 2, 1977, September 26, 1977 and November 10, 1977): second by Olsen et al. in USA, and the third set by Arjis et al. (1978). The results in these three sets are not identical; furtheremore, there are distinct differences between the balloon measurements of Arnold et al. and their earlier

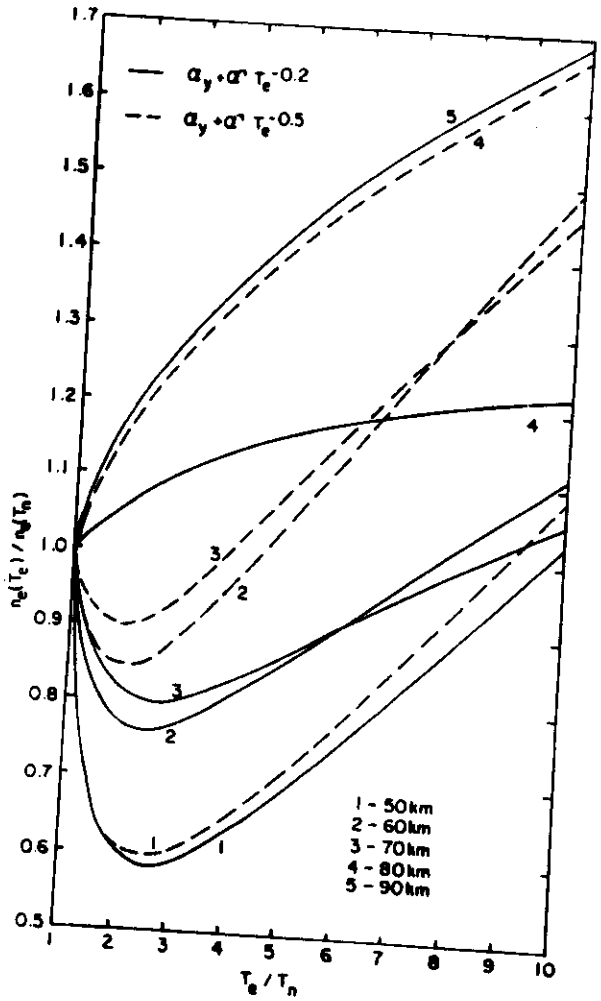

FIG. 10. Effect of HF heating of the D-region. The changes in electron density are given as a function of increase in electron temperature. Note that in the lower D-region, the electron density decreases up to $T_e = 700°K$.

rocket measurements. For example, the nature of ion seen is substantially different and the NPH fractional abundance is considerably lower in the balloon flights than in the earlier rocket flights. Its value for the more recent balloon flights was:

Fractional abundance of NPH = 0.43 at 37 km.

A comparative listing of the ions seen in these different balloon and rocket flights as well as possible identification of these ions (the basis of the identification will be discussed later) are given in Table 1.

It is believed that PH to NPH conversion occurs through the following reaction:

$$H^+(H_2O)_n + X \rightarrow H^+X(H_2O)_{n-m} + mH_2O$$

where X is a minor constituent to be identified and m depends on the difference of proton affinities of X and H_2O. One can derive the threshold concentration of X by writing:

$$k[PH^+][X] = \alpha_i N^-[NPH^+]$$

Arnold et al. used $\alpha_i = 5 \times 10^{-8}$ cm^3 s^{-1} and $k = 10^{-9}$ cm^3 s^{-1}. The right-hand side then is roughly 10^{-3}. This means that the unknown reaction partner X for PH should have a concentration larger than 6×10^6 cm^{-3}. In an earlier work, when only the rocket observations were available, Arnold et al. believed that this unknown minor constituent X is perhaps CH_2O.

Subsequently after the balloon measurements were carried out, they suggested X to be CH_3CN. Arnold et al. concluded the following:

$X = 41 \pm 1$ a.m.u.

$\tau_{ion} = 7000$ sec ($\alpha_i \sim 7.5 \times 10^{-8}$ cm^3 s^{-1} and $n^- = 2 \times 10^3$ cm^{-3})

$$\tau_{PT}(PH \rightarrow NPH) = (k[X])^{-1} = \frac{5 \times 10^8}{[X]}$$

$$\frac{[H^+X(H_2O)_b]}{[H^+(H_2O)_n]} = 1.4 \times 10^{-5}\,[X]$$

$[X] = 7 \times 10^4$ cm^{-3}

Mixing ratio of $X = 7 \times 10^{-13}$

Proton affinity of $X \gtrsim 175$ KCAL MOL^{-1}

However, a re-examination of these ions by Ferguson (1978) has led Ferguson to believe that the unknown minor constiment is NaOH. The consequences are the following:

$$X \equiv NaOH$$

proton affinity = 248 KCAL MOL^{-1}

$$[NaOH] = 10^5\ \text{cm}^3$$

$$H^+(H_2O)_n + NaOH \rightarrow NaOH_2^+(H_2O)_m + (n\text{-}m)H_2O \quad \text{Reaction fast}$$

The identification of the ions on these basis is also indicated in Table 1.

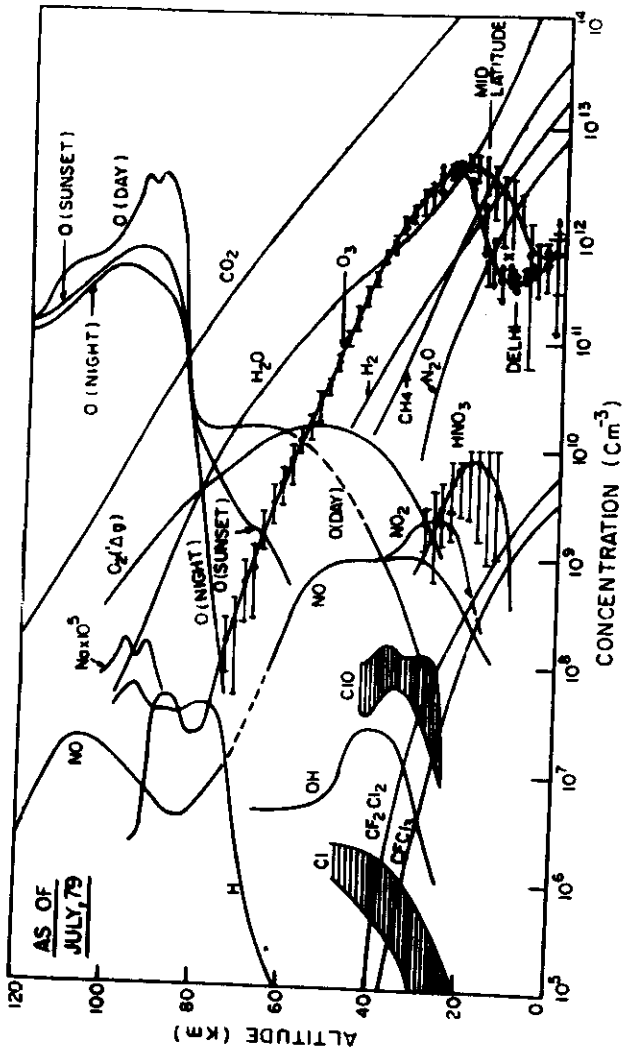

Fig. 11. A Reference Model of Atmospheric minor constituents in the Middle Atmosphere. The profiles are based on experimental data from a wide variety of sources.

3.2. *Stratospheric Negative Ions*

3 sets of balloon flights were conducted by Arnold and Henschen (1978) on September 2, 26 and Nov. 10, 1977. The uncertainty in the measurements was ± 3 AMU.

The theoretical expectation of Ferguson (1979) and the tentative identifications of Arnold and Henschen are given in Table 2.

3.3. *Role of Ions on Minor Neutrals in the Stratosphere*

The ionic concentrations in the stratosphere are around 10^3 cm^{-3} and this is equivalent to a minor neutral concentration of 10^6 cm^{-3}. At times when these ionization densities are greatly enhanced as during particle events following solar flare, their roles become comparable to neutral processes, especially through ion-ion recombination process generating active HO_x and NO_x (see below).

In examining such role it is instructive to compare the time τ_x taken by an ion to combine with a trace constituent as against the time taken for ion-ion recombination τ_i. This obviously is going to be different for different trace species. Where $\tau_x < \tau_i$ it is obvious that the role of ions on minor species may begin to become important; also clustering of this kind has obvious bearing on ion composition and nucleation. For such calculations one must have a reasonable reference model for trace constituents — one is given in Fig. 11.

3.3.1. *Ion Combination with Trace Constituents*

An example is given in Table 3; this represents the conditions at 20 km. The ion-ion recombination line for a 2-body process is about 8000s, but can be as short as 25s where aerosol ions of giant sizes are involved.

3.3.2. *Positive Ions and Electrons*

Production H/OH can occur through dissociative reactions:

(1) $H_3O^+(H_2O)_n + e \rightarrow (n+1)H_2O + H \quad (7.4 \pm 1.5) \times 10^{-6}$ for $n=4$

$\rightarrow H_2 + OH + nH_2O \quad (9.2 \pm 2.0) \times 10^{-6}$ for $n=5$

Swider and Keneshea (1972) have pointed out that the normal O_2^+ clustering chain produces OH or H for every O_2^+ hydration through the sequences

(2) $$O_2^+ \rightarrow O_4^+ \rightarrow H_3OH^+ \xrightarrow{H_2O} H_3O_2^+ + OH$$

Thus for every O_2^+ conversion to an oxonium ion, one OH molecule is generated. Since 90 % of all ionization by energetic particles by air will yield O_2^+ ion, this means that OH production rate through (2) is equal to q.

Considering (1) and (2) together;

Ionic Production of H/OH $\leq 2q$

Swider and Keneshea (1972) hace considered processes (1) and (2) for mesospheric OH/H production vis-a-vis neutral production through:

$$O(^1D) + H_2O \rightarrow 2OH$$
$$H_2O + h\beta \rightarrow H + OH$$

for a PCA event.

In the stratosphere, N_e is negligiable and so H/OH production through (1) is negligible. Hence here,

$$P_i(OH, H) \sim q$$

3.3.3. *Positive Ion Clustering with CFM's*

Possible loss of CFM's (F-11 and F-12) through reaction with $H_3O^+(H_2O)_n$ has been investigated by Fehsenfeld et al. (1976). The following possibilities arise:

(3) $H_3O^+(H_2O)_n + CFCl_3 \rightarrow$ Products $\left\{ \begin{array}{l} 4\times10^{-10} \text{ for } n=0 \\ <10^{-12} \text{ for } n=1 \\ <10^{-13} \text{ for } n=2,3 \end{array} \right.$

(4) $H_3O^+(H_2O)_n + CF_2Cl_2 \rightarrow$ Products not observed to occur for $n=0,1,2,3$

(5) $NH_4^+(H_2O)_n + CFCl_3 \rightarrow$ Products

(6) $NH_4^+(H_2O)_n + CF_2Cl_2 \rightarrow$ Products

For reactions of category (4), none is observed to occur. Even for H_3O^+, the reaction rate is $<10^{-12}$ cm^3/s.

For (5) the rate is $<4\times10^{-13}$ and for (6) $<2\times10^{-11}$ cm^3/s.

Production of $NH_4^+(H_2O)_n$ or $NH_4^+(NH_3)_n(H_2O)_w$ ions occur through:

(7a) $H_3O^+(H_2O)_n + NH_3 \rightarrow NH_4^+(H_2O)_{n-m} + (m-1)H_2O$

(7b) $NH_4^+ NH_3(H_2O)_w + H_2O \rightarrow NH_4^+(NH_3)_n(H_2O)_{w+1}$ $\sim10^{-9}$ cm^3/s (Clustering Reaction)

(8) $H_3O^+(H_2O)_3 + NH_3 \rightleftharpoons NH_4^+(H_2O)_2 + H_2O$

followed by:

(9a) $NH_4^+(H_2O)_w \rightarrow NH_4^+(H_2O)_{w-1} + H_2O$

(9b) $NH_4^+(H_2O)_n + HCl \rightarrow H_3O^+(H_2O)_{n-1} + NH_4Cl$

(9c) $NH_4^+(NH_3)_{n-1}(H_2O)_w + NH_3 \rightarrow NH_4^+(NH_3)_n(H_2O)_w$

and consequently these have no net effects on the positive ion system excepting in removing HCl. Furthermore, it is unlikely that NH_3 concentration is large enough to have any appreciable part in the ionic sequence.

Thus the only reaction that needs to be kept in view, if Fehsenfeld et al. (1976) results above are considered, is:

$$H_3O^+ + CFCl_3 \rightarrow \text{Products}$$

Even for this, since H_3O^+ is an intermediate ion in the clustering sequence of O_2^+ and its concentration is small, loss of $CFCl_3$ by this process is negligible.

3.3.4. *Ion-Ion Sequences*

The terminal negative ions will combine with positive ions yielding HNO_3 and HO_x through the reactions:

(10) $NO_3^-(H_2O)_n + H_3O^+(H_2O) \xrightarrow{M} HNO_3 + (n+m)H_2O$

(10a) $NO_3^-(H_2O)_m + NH_4^+(H_2O)_n \xrightarrow{M} NH_4NO_3 + (n+m)H_2O$

(11) $CO_{3,4}^-(H_2O)_n + H_3O^+(H_2O)_n \rightarrow NO_x$

Process (10) takes an active NO_x out of circulation and generates an inactive HNO_3 in the sequence.

Process (11), presumably applicable at night when terminal ions are O_4^-, CO_3^- or CO_4^-, introduces an active NO_x species in the system.

3.3.5. *Direct Attack on O_3*

There are several reactions of negative ions which directly deplete ozone. These may be described by:

(12) $X^- + O_3 \rightarrow XO^- + O_2$

However, the only reasonably fast reaction of this kind is

(13) $NO_2^- + O_3 \rightarrow NO_3^- + O_2 + 2.2$ ev $\quad (1.8\times10^{-11})$

For NO_3^-, the rate is found to be less than 2×10^{-12} cm^3/s: and for the terminal negative ions, the rate is not known. NO_2^- being an intermediate ion with a low concentration is of little consequence.

Ruderman, Foley and Chamberlain (1976) have examined the catalytic destruction of ozone in the polar region using the following reaction:

$$NO_3^- + O_3 \rightarrow NO_2^- + 2O_2 + 0.8 \text{ ev}$$

He also suggests that a similar cycle may proceed though ClO_x^- and ClO_{x-1}^-. Polar ozone (with seasonal variations averaged) will be governed by the equation:

$$-\frac{d}{dt}[O_3] = S - (\alpha + \beta\cos\omega t)[O_3]$$

in which S is an approximately constant source term (including divergence of O_3 flow from other regions), α is the rate of O_3 outflow from the polar region plus its destruction rate, $2k_2[NO_3^-]_o$, where $[NO_3^-]_o$ is the mean ion density and $\beta = 2k_2\Delta[NO_3^-]$.

Assuming for 20 km in polar region

$[NO_3^-]_o = 6.0\times10^3$ cm^{-3}

$[NO_3^-] = 0.7\times10^3$ cm^{-3}

75

76

they concluded that the reported polar cap ozone variation of about 6 percent between maximum and minimum solar activity is obtained for $k_2 = 3\times10^{-12}$ $cm^{-3}\,s^{-1}$ and for the outflow time of total ozone (τ) = 3 months. However, as we have pointed out before, this requirement of 3×10^{-12} cm^3/s is larger than observed in the laboratory.

Other reactions that may be considered and for which reaction rates are available include the following:

$$CO_4^- + O_3 \rightarrow O_3^- + O_2 + CO_2 \qquad (1.3\times10^{-10})$$
$$O_2^-(H_2O)_n + O_3 \rightarrow \text{Products} \qquad (2\times10^{-10})$$

3.3.6. *Dissociative Attachment of CCl_4, $CFCl_3$ and CF_2Cl_2*

Another type loss process for Chlorine compounds is the following:

$$CCl_4 + e \rightarrow \text{products} \qquad (4.1\times10^{-7})$$
$$CFCl_3 + e \rightarrow \text{products} \qquad (1.4\times10^{-7})$$
$$CF_2Cl_2 + e \rightarrow \text{products} \qquad (2.4\times10^{-9})$$

However, attachment loss rates through these processes (given by $k[X]$) are a thousand times smaller than loss by attachment to O_2.

3.3.7. *Negative Ions and CFMS*

The following processes have been considered by Fehsenfeld and Ferguson (1974):

$$\left.\begin{aligned} CO_3^- + CF_2Cl_2 &\rightarrow \text{products} \\ CO_3^- + CFCl_3 &\rightarrow \text{products} \\ NO_3^- + CF_2Cl_2 &\rightarrow \text{products} \\ NO_3^- + CFCl_3 &\rightarrow \text{products} \end{aligned}\right\} \text{ all slow}$$

$$O_2^- + CF_2Cl_2 \rightarrow Cl^- + CF_2Cl + O_2 \qquad (2.1\times10^{-10})$$
$$O_2^- + CFCl_3 \rightarrow Cl^- + CFCl_2 + O_2 \qquad (7.6\times10^{-10})$$
$$O_2^-(H_2O) + CF_2Cl_2 \rightarrow \text{products} \qquad (<1\times10^{-11})$$
$$O_2^-(H_2O)_2 + CF_2Cl_2 \rightarrow \text{products} \qquad (<1\times10^{-13})$$
$$O_2^-(H_2O)_3 + CF_2Cl_2 \rightarrow \text{products} \qquad (<1\times10^{-13})$$
$$O_2^-(H_2O)_n + CFCl_3 \rightarrow \text{products} \qquad (<10^{-11} \quad (n=1)$$
$$<10^{-13} \quad (n=2,3))$$

Also $NO_2^- + HCl \rightarrow Cl^- + HNO_3 \qquad (1.4\times10^{-9})$

followed by:

$$Cl^- + HNO_3 \rightarrow NO_3^- + HCl \qquad (1.6\times10^{-9})$$

or $Cl^- + Cl^-(H_2O)_n + H^+(H_2O)_n \rightarrow HCl + (n+m)H_2O$ (releasing HCl)

Cl^- ions have been observed in the Ionosphere. ClX^- should be important in the stratosphere.

3.3.8. *Ions and Aerosols*

We are concerned with the following types of effects:

(a) Combination of small ions with aerosols (charged and uncharged) for which the coefficient is b.

(b) Combination of small ions with uncharged aerosols for which the coefficient is γ_0.

(c) Ion-ion recombination involving aerosols ions, including:

  (a) positive aerosol ions with negative aerosols ions

  (b) positive aerosol ions with $NO_3^-(H_2O)_n$ or $CO_4^-(H_2O)_n$

  (c) negative aerosol ions with $N_3O(H_2O)_n$.

Dixon and Jennings (private communication) from experimental measurements of small ion decay with submicrometer aerosol particles, found:

Ion-ion repulsion coefficient	: $2.39 \pm 0.14\times10^{-6}$ cm^3/s (from 14 plots of small ion decay)
Combination coefficient of small ions with aerosols (b)	: 0.30 to 2.24×10^{-6} for $r = 1.26\times10^{-6}$ to 4.0×10^{-6} cm^3/s
Combination coefficient of small ions with uncharged aerosols (γ_0)	: 0.39 to 2.34×10^{-6} for $r = 1.26\times10^{-6}$ to 4.0×10^{-6} cm^3/s

Hoppell (1974) found experimentally:

$$b \propto r^{1.22}$$

in comparison to the theoretical value of

$$b \propto r^{1.17}$$

The continuity equation for aerosol ions is given by:

$$\frac{dn^{+,-}}{dt} = q - \alpha_i n^+ n^- - n^{+,-}\int_{r_{min}}^{r_{max}} \beta(r)\, f(r)\, dr$$

where β is the ion-annihilation coefficient with atmospheric aerosols,
$f(r)$ is the aerosol size distribution,
r is the radius of the aerosol particles,
α_i is the ion-ion recombination coefficient,

Zikmunda and Mohnen (1972) have evaluated $\int \beta(r) f(r) dr$ for the stratosphere and found it to be much smaller than the ion loss due to recombination for the unperturbed stratospheric particle lead. This is, however, in conflict with the general belief that presence of aerosols depletes the concentration of small ions and that occasional depletions seen in positive ion profiles is, in fact, a measure of aerosols. Later we shall see this is indeed the case under certain conditions.

77

78

4. Troposphere - Stratosphere - Mesosphere Scheme

We have used two approaches: in the first, complete negative and positive ion sechemes are used with the addition of a set of reactions involving aerosols both in negative and positive ion sequences; in the second the 6-ion simplified model used by us earlier (the so-called unified scheme which has been found to be fairly effective over a wide variety of conditions in the mesosphere including solar flares, eclipse and PCA's) has been expanded in the light of criteria listed in Introduction.

We will discuss here only this simplified but expanded scheme. The scheme is given in Fig. 12. This scheme has been used sometimes in conjunction with a more complex clustering sequence of positive ions given in Fig. 13 when details of ion composition in the stratosphere becomes the main interest. The different possibilities of PH to NPH conversion are shown in this diagram. Where the exact composition of ion is not required and the interest is mainly in determining the effect of minor constituents on the ionic concentrations (as in the case of aerosols, producing localised depletions), or where only one clustering channel is believed to operate for PH to NPH conversion through a minor constituent X whose identity and concentration are required to be determined, or where one wishes to know the rate of production of HO_x and NO_x through the ionic reaction as an input to ozone chemistry, we believe the simplified scheme is adequate. Furthermore in understanding the roles played by the different factors, the simplified scheme has an advantage. The more complex negative ion scheme, which we have also occassionally used, is not reproduced here.

When aerosol effects are considered, then the scheme of Fig. 9 is taken as it is, with aerosol profiles taken from experimental observations wherever possible. The ones we have taken are given in Fig. 14. If we are not concerned with the aerosol process but are considering the possibility of PH to NPH conversion through an unknown minor constituent X, then in the scheme aerosols are replaced by X (Fig. 12) and β^- and β^+ are appropriately altered. Thus the differences between the involvement of aerosols and of minor constituents of the type CH_3CN or NH_3 or NaOH etc. are that in the latter, all the four ion-ion recombination coefficients are equal and are appropriate for small ions, whereas in the former two body component varies from $7\times10^{-8}\ cm^3\ s^{-1}$ for α_{11} to $2\times10^{-6}\ cm^3\ s^{-1}$ for α_{22}.

It is also important to remember that the ion-ion recombination coefficient is no longer limited to two body process that we use for the mesospheric heights. We have to use the expression of the type

$$\alpha_i = \alpha(2\ \text{body}) + \alpha(3\ \text{body})$$
$$= \alpha(2\ \text{body}) + 2\times10^{-(25+0.5)}\left(\frac{T}{300}\right)^{-0.5}$$

For the two body component, the value is taken to be $6\times10^{-8}\left(\frac{T}{300}\right)^{0.5}\ cm^3\ s^{-1}$

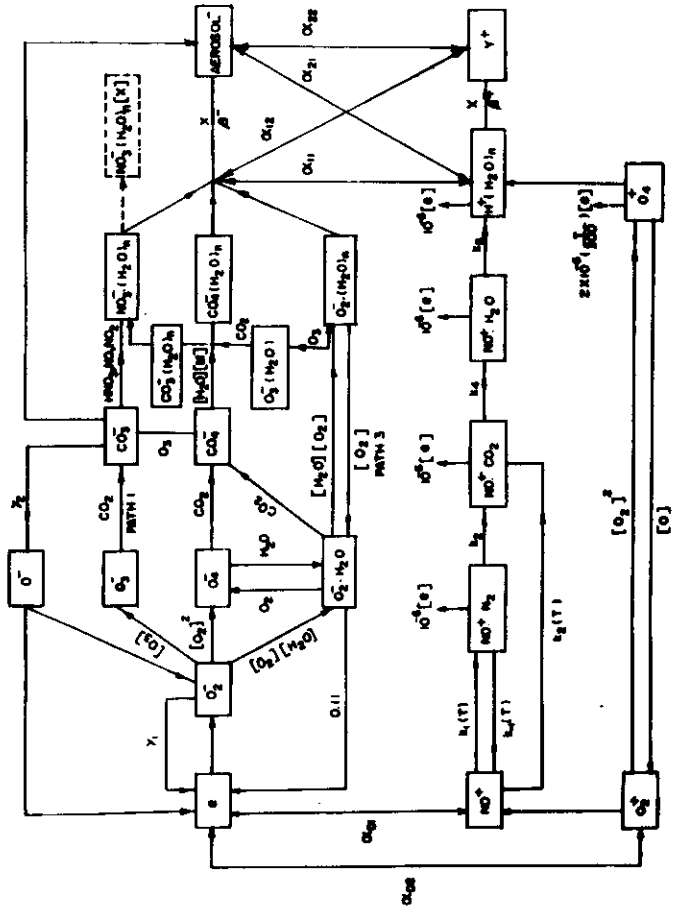

Fig. 12. An extended ion scheme that can be used for the entire middle ionosphere. The scheme also includes possible interaction of aerosols as well as conversion of proton hydrates to non-proton hydrates.

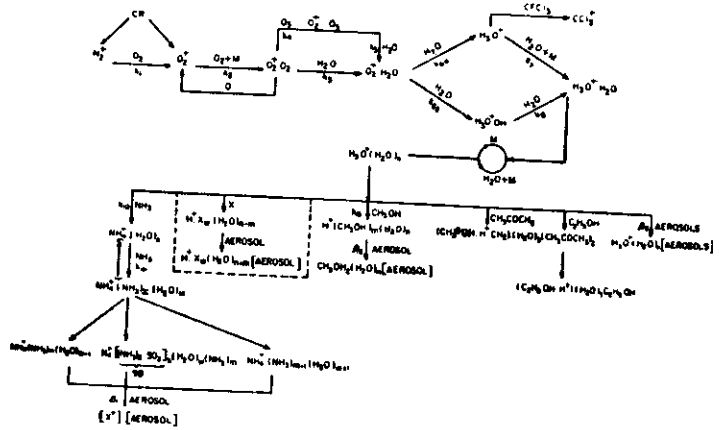

FIG. 13. Detailed scheme of positive ion sequences in the Stratosphere. Note the different clustering sequences.

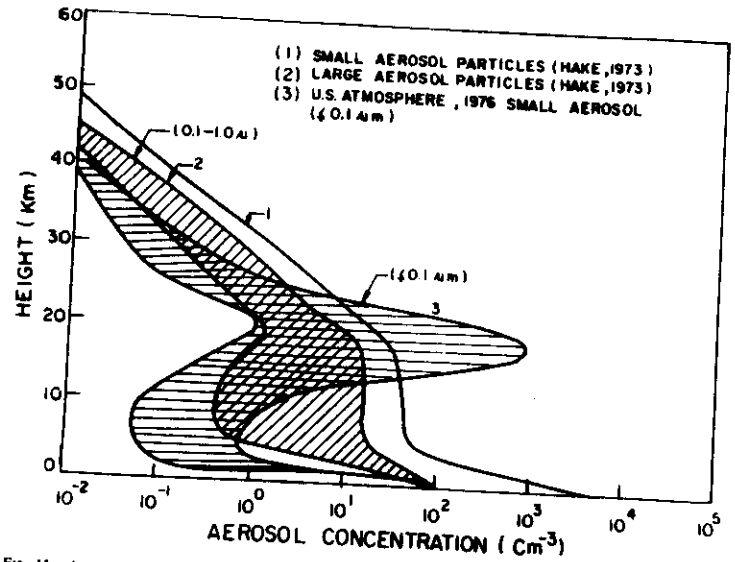

FIG. 14. Aerosol profiles in the Troposphere and Stratosphere. Profile 1 is that given by Hake et al. (1973) for small (Aitken) particles and profile 2 for large (0.1-1.5 m) particles. The shaded regions are those given by US Standard Atmosphere 1976.

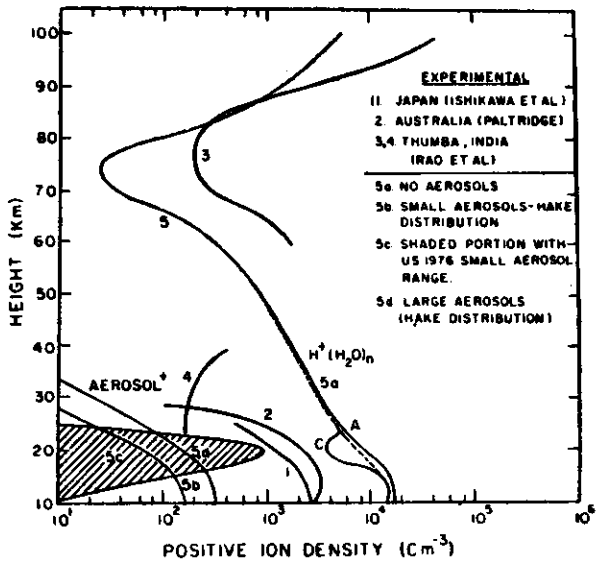

FIG. 15. Calculated change in positive ion density with aerosol distributions given in Fig. 14. The calculation are made with the ionic scheme of Fig. 13.

for processes involving $CO_{3,4}^-(H_2O)_n$ or $NO_3^-(H_2O)_n + H_3O^+(H_2O)_n$. For aerosol particles the two body component is taken to be 2×10^{-6} cm^3 s^{-1}. For the combination coefficient, given by β, we use the values obtained recently by Dixon and Jennings. A short summary of these are given in Table 4.

Another important input is q(CR), the ion production rate due to galactic cosmic rays. If the role played by aerosols has to be properly examined, then q(CR) must be known with a good deal of accuracy. As we shall see later when there is a strong layer of aerosols, the effect is a distinct hole in the ion profile which is easily measurable. However in case of monotonically varying distribution of aerosol particles, the ion concentration that one would have obtained in the presence of aerosols differs from one that one would have obtained in the absence of it by an amount which is not very large and should exceed the error involved in the use of q(CR) values. The conclusion by Zikmunda and Mohnen (1972) that the aerosol attachment term is negligible and the conflicting belief amongst the Japanese workers that there is a distinct and measurable difference between the observed ion concentration and the expected value, rest primarily on how well one can determine q(CR). The values that we have used in this work are those recently synthesised by Heaps (1978).

When we use the scheme in the presence of aerosols of the type given in Fig. 14, we get the positive ion distribution shown by the curve 5C in Fig. 15. The monotonic distribution of aerosols given by Hake (1973) are shown by the dotted line and no-aerosol case is shown by the solid line. It is clear that an aerosol layering of the type given by US 1976 Model will produce a distinct and a large ion hole that should be easy to measure. Thus by measuring possible ion concentration in the stratosphere, one should be in a position to determine the aerosol concentrations provided some assumption is made about the aerosol size. The scheme gives some additional information also. For example, we can determine from the magnitude of the observed hole in n^+, the concentration of large aerosol ions which should be the precursor for nucleation processes. Curves 5B, 5C and 5D show values of these large aerosol ions for the three aerosol distributions.

The next step is to find out, by coupling the ion scheme to an ozone scheme, to what extent the different ionic processes contribute to neutral minor constituent chemistry, in particular, the chemistry involving ozone. In Table 4 we give a list of the reactions that have such an effect.

In regard to the direct ozone loss with negative ions, the possibilities do not appear to be very encouraging. But neverthless this matter is not closed. The only reaction which appears to be reasonably fast is one given in equation 17 involving NO_2^- in which the reaction rate is 1.8×10^{-11} cm^3 s^{-1}. NO_2^- being an intermediate ion, this reaction has no such significance. As we have also indicate before, the rate is found to be less than 10^{-12} cm^3 s^{-1} for NO_3^- but again this informations is not of much significance, since what we are really concerned

with are the rates for reactions involving $NO_3^-(H_2O)_n$, $CO_{3,4}^-(H_2O)_n$ or $O_2^-(H_2O)_n$. It is important to note that $O_2^-(H_2O)_n + O_3$ products is reported to be fast ($\sim2\times10^{-10}$ cm^3/s) and since $O_2^-(H_2O)_n$ ions are likely to be dominant in the troposphere, such processes cannot be entirely ignored.

The next term (PH to NPH conversion) is of importance in understanding the nature of ion composition but is unlikely to have any effect on the minor neutral chemistry.

The reactions which are likely to be important (especially during SPE's are the 4th, 5th, 7th and the 8th reactions in the table. Dissociative recombination of proton hydrates with electrons and conversion of H_3O^+ to $H_5O_2^+$ produce HO_x molecules which are active components in the ozone cycle. Where Ne is not negligible, the two together generate 2(OH) per ion pair. If the ion production increases as during pronton flare events or during supernova explosions we have corresponding increases in OH production rate with significant effects on ozone concentration. Thus solar proton events effect the ozone chemistry not only through the production of nitric oxide (the 8th reaction in Table 4, and the one that has been considered in the interpretation of August 1972 case by Heath, Crutzen and Reid) but also through increased OH production through the channel $O_2^+ \rightarrow H_3O^+ \rightarrow H_5O_2^+$. Thus solar proton events should be operating in a two fold path, only one of which has been considered in the past.

Acknowledgement

The preparation of this article was done during my tenure as a Jawaharlal Nehru Fellow. Part of the material presented here arose from my visit to NCAR during October-November, 1979.

TABLE 1. POSITIVE ION COMPOSITION IN THE STRATOSPHERE

IDENTIFICATION NPH	IDENTIFICATION PH	BALLOON (ARNOLD)	ROCKETS (ARNOLD)	BALLOONS (ARJIS)	BALLOON (OLSEN ETAL)	IDENTIFICATION BY FERGUSON
	$H^+(H_2O)$		19			
ROCKET	$H^+(H_2O)_2$		29 ± 2			
42 H^+X			37 ± 2			
60 $H^+X(H_2O)$	$H^+(H_2O)_3$	55 ± 1	42 ± 2	42 ± 3		
Probably fragmentation of $H^+X(H_2O)_2$	$H^+(H_2O)_4$	73 ± 1 By far the most abundant	55 ± 1 60 ± 2 73 ± 1	60 ± 2		41 $NaOH_2^+$
$H^+X(H_2O)_2$		78 ± 1	80 ± 2	78 ± 2, 82 ± 2		59 $NaOH_2^+H_2O$
	$H^+(H_2O)_5$	91 ± 1				77 $NaOH_2^+2H_2O$ 81 $NaOH_2^+NaOH$
$H^+X(H_2O)_3$		96 ± 1 Most abundant		96 ± 2		
$H^+X_2(H_2O)$		100 ± 1		99 ± 2		95 $NaOH_2^+3H_2O$
	$H^+(H_2O)_6$?			109 ± 2 ($H^+(H_2O)_6$?		99 $NaOH_2^+NaOH\ H_2O$
$H^+X(H_2O)_4$		114 ± 2				115 $NaOH_2^+4H_2O$
$H^+X_2(H_2O)_2$		118 ± 1				
$H^+X_2(H_2O)_3$		136 ± 2				117 $NaOH_2^+NaOH\ 2H_2O$ 135 $NaOH_2^+NaOH\ 3H_2O$
$H^+X_3(H_2O)$		140 ± 2				139 $NaOH_2^+NaOH\ H_2O$

$H^+(H_2O)_n + X \rightarrow H^+X(H_2O)_{n-m} + mH_2O$

TABLE 2. NEGATIVE IONS IN THE STRATOSPHERE

A. THEORETICAL POSSIBILITIES

$NO_3^-X(H_2O)_n$
$CO_3^-X_2(H_2O)_n$
$O_2^-X_3(H_2O)_n$
eg. $NO_3^-(H_2O)_n(SO_3)_m(HNO_3)_l$ (Ferguson, 1979)

B. ARNOLD-HENSCHEN MEASUREMENTS

Observed mass number	*Tentative identification*
125 ± 2	$NO_3^-HNO_3$
161 ± 2	R^-HNO_3
188 ± 2	$NO_3^-HNO_3HCl$
	$NO_3^-(HNO_3)2$
197 ± 3	R-HR
224 ± 3	$R^-(HNO_3)_2$
253 ± 3	$NO_3^-(HNO_3)_2$
260 ± 3	R-HR HNO_3
289 ± 3	$R^-(HNO_3)3$
	$NO_3^-(HNO_3)3HCl$
295 ± 3	$R^-(HR)_2$

Three sequences

1) $NO_3^-(HNO_3)_n$ n = 1,2,3
2) $NO_3^-(HCl)(HNO_3)_n$ HR = 98 ± 2
3) $R^-(HR)_m(HNO_3)_n$ m + n 3
HR H_2SO_4 or $HClO_4$

TABLE 3. CHARACTERISTIC ION INTERACTION TIMES AT 20 KM

2-BODY	$\tau_i \sim 8000$	SMALL IONS
2-BODY+	$\tau_i \sim 600$	SMALL IONS
3-BODY	$\tau_i \sim 25$	LARGE IONS

Trace constituent		*Ion interaction time with trace constituent*
O_3	4×10^{12} cm^{-3}	10^{-4} s
HNO_3	8×10^{9}	6×10^{-2} s
HCl	2×10^{9}	2.5×10^{-1} s
ClO	(10^{6})	(500s) TOO LARGE
OH	(5×10^{5})	(5000s) TOO LARGE
SO_2	4×10^{8}	1
H_2SO_4	$(10^{5}-10^{8})$	(5000-5s) LARGE (?)
NH_3	$<10^{9}$	>0.2 s
CF_2Cl_2	3×10^{8}	2 s
$CFCl_3$	10^{8}	5 s
CH_4	2×10^{12}	2.5×10^{4} s

87

TABLE 4. IONIC REACTIONS OF INTEREST IN NEUTRAL CHEMISTRY

Direct O_3 loss	$X^- + O_3 \rightarrow XO$	
PH → NPH	CH_2O, HCN, CH_3OH, NH_3, C_2H_5OH, CH_3CN, NaOH etc.	
PH → Aerosol Clustering	Aerosols → X⁻[Aerosol] (Decrease in Measured Ion Concentrations)	
PH + e	H/OH Production (Active Components in O_3 Cycles)	
$H_3O^+ \rightarrow H_3O_2^+$	OH Production (Active Components in O_3 Cicles) (total 2[OH] per ion pair)	
$H_3O^+(H_2O)_n + NO_3^-(H_2O)_n \rightarrow HNO_3$ (Inactive)		
$C_{3,4}^-(H_2O)_n + H_3O^+(H_2O)_n \rightarrow HO_x$ (Active)		
GCR / SPE → NO		No Production (Active component in O_3 cycle) (13 NO molecules per Ion pair).

88

REFERENCES

ARJIS, E., INGLES, J. and NAVEJAS, D.: Nature, *271*, 642, 1978.
ARNOLD, F., BÖHRINGER, H. and HENSCHEN, G.: Geophys. Res. Lett., *5*, 653, 1978.
ARNOLD, F. and HENSCHEN, G.: Nature, *257*, 521, 1978.
DIXON, A. M. and JENNINGS, S. G.: Private Communication.
FEHSENFELD, F. C. and ALBRITTON: Geophys. Res. Lett., *4*, 61, 1977.
FEHSENFELD, F. C. and FERGUSON, E. E.: J. Chem. Phys., *61*, 3181, 1974.
FEHSENFELD, F. C., CRUTZEN, P. J., SCHMELTEKOPF, A. L., HOWARD, C. J., ALBRITTON, D. L., FERGUSON, E. E., DAVIDSON, J. A. SCHIFF H. I.: J. Geophys. Res., *81*, 4454, 1976.
FERGUSON, E. E.: Geophys. Res. Lett., *5*, 1035, 1978.
FERGUSON, E. E.: *Middle Atmosphere Electrodynamics*, ed. N.C. Maynard NASA, 1979.
HAKE, R. D. Jr, PIERCE, E. T. and VIEZEE, W.: Stratospheric Electricity, Final Report SRI Project 1724, Stanford Research Institute, Menlo Park, Calif., 1973.
HEAPS, M. G.: Planet. Space Science, *26*, 513, 1978.
HEATH, D. F., KRUEGER, A. J. and CRUTZEN, P. J.: Science, *197*, 886, 1977.
HOPPEL, W. A.: PAGEOPH, *81*, 230, 1970.
MITRA, A. P. and ROWE, J. N.: J. Atmosph. Terr. Phys, *34*, 795, 1972.
MITRA, A. P.: J. Atmosph. Terr. Phys., *37*, 895, 1975.
ROWE, J. N., MITRA, A. P., FERRARO, A. N. and LEE, H. S.: J. Atmosph. Terr. Phys., *36*, 755, 1974.
RUDERMAN, M. A., FOLEY, H. M. and CHAMBERLAIN, J. W.: Science, *192*, 555, 1976.
SWIDER, W. and KENESHEA, T. M.: Planet. Space Science, *21*, 1969, 1973.
TOMKO, A. A., FERRARO, A. J., LEE, H. S. and MITRA, A. P.: J. Atmosph. Terr. Phys., *42*, 275, 1980.
ZIKMUNDA, J. and MOHNEN, V. A.: Meteorologische Rundshau, *25*, 10, 1972.

89